JPn Neuroscience
The Journal of Physiology

Virtual leak channels modulate firing dynamics and synaptic integration in rat sympathetic neurons: implications for ganglionic transmission *in vivo*

Mitchell G. Springer, Paul H. M. Kullmann and John P. Horn

Department of Neurobiology and Center for Neuroscience, University of Pittsburgh School of Medicine, Pittsburgh, PA, USA

Key points

- The synaptic organization of paravertebral sympathetic ganglia enables them to relay activity from the spinal cord to the periphery and thereby control autonomic functions, including blood pressure and body temperature.
- The present experiments were done to reconcile conflicting observations in tissue culture, intact isolated ganglia and living animals. By recording intracellularly from dissociated neurons and intact ganglia, we found that when electrode damage makes cells leaky it could profoundly distort cellular excitability and the integration of synaptic potentials.
- The experiments relied on the dynamic clamp method, which allows the creation of virtual ion channels by injecting current into a cell based upon a mathematical model and using rapid feedback between the model and cell.
- The results support the hypothesis that sympathetic ganglia can produce a 2.4-fold amplification of presynaptic activity. This could aid understanding of the neural hyperactivity that is believed to drive high blood pressure in some patients.

Abstract The excitability of rat sympathetic neurons and integration of nicotinic EPSPs were compared in primary cell culture and in the acutely isolated intact superior cervical ganglion using whole cell patch electrode recordings. When repetitive firing was classified by Hodgkin's criteria in cultured cells, 18% displayed tonic class 1 excitability, 36% displayed adapting class 2 excitability and 46% displayed phasic class 3 excitability. In the intact ganglion, 71% of cells were class 1 and 29% were class 2. This diverges from microelectrode reports that nearly 100% of superior cervical ganglion neurons show phasic class 3 firing. The hypothesis that the disparity between patch and microelectrode data arises from a shunt conductance was tested using the dynamic clamp in cell culture. Non-depolarizing shunts of 3–10 nS converted cells from classes 1 and 2 to class 3 dynamics with current–voltage relations that replicated microelectrode data. Primary and secondary EPSPs recorded from the intact superior cervical ganglion were modelled as virtual synapses in cell culture using the dynamic clamp. Stimulating sympathetic neurons with virtual synaptic activity, designed to replicate *in vivo* recordings of EPSPs in muscle vasoconstrictor neurons, produced a 2.4-fold amplification of presynaptic activity. This gain in postsynaptic output did not differ between neurons displaying the three classes of excitability. Mimicry of microelectrode damage by virtual leak channels reduced and eventually obliterated synaptic gain by inhibiting summation of subthreshold EPSPs. These results provide a framework for interpreting sympathetic activity recorded from intact animals and support the hypothesis that paravertebral ganglia function as activity-dependent amplifiers of spinal output from preganglionic circuitry.

DOI: 10.1113/jphysiol.2014.284125

(Received 8 September 2014; accepted after revision 4 November 2014; first published online 8 November 2014)
Corresponding author J. P. Horn: Department of Neurobiology and Center for Neuroscience, University of Pittsburgh School of Medicine, E1440 Starzl Biomedical Science Tower, Pittsburgh, PA 15261, USA. Email: jph@pitt.edu

Abbreviations AHP, afterhyperpolarization; C_m, membrane capacitance; E_{leak}, leak equilibrium potential; E_{rev}, reversal potential; *f–I*, frequency–current; f_{post}, postsynaptic firing frequency; f_{pre}, presynaptic firing frequency; g_{leak}, leak conductance; g_{syn}, synaptic conductance; I_A, A-type K^+ current; I_M, M-type K^+ current; I_{syn}, synaptic current; *I–V*, current–voltage; L3, third lumbar; NGF, nerve growth factor; R_{in}, input resistance; SCG, superior cervical ganglion; thresh-g_{syn}, threshold synaptic conductance; *s*, synaptic scaling constant; t_{sum}, temporal window of summation; V_m, membrane potential; V_{rest}, resting membrane potential; ZAP, swept sine wave.

Introduction

The capacity of neurons to integrate postsynaptic activity depends upon their intrinsic excitability. Cells regulate action potential generation and the dynamics of repetitive firing by selectively expressing specific combinations of ion channels (Hille, 2001). Because of specialized neuronal firing dynamics, distinct cell types in various brain regions may respond differently to similar patterns of synaptic activity. In this way, sustained depolarization can drive different neurons either to steady repetitive firing, brief transient firing, repeated bursts of spikes or to a large repertoire of more complex temporal firing patterns (Prinz *et al.* 2004; Izhikevich, 2007). The cellular diversity of excitability is important because it helps to implement the computations performed by different neural circuits. In addition, the classification of action potential patterns elicited by depolarizing stimuli can provide practical experimental signatures for cell identification. Here we examine the intrinsic excitability of sympathetic neurons in the paravertebral superior cervical ganglion (SCG) of the rat and the implications for integrative synaptic amplification in this circuit.

Previous studies of autonomic neurons have classified them as either phasic or tonic. Phasic neurons typically fire one or two action potentials in response to depolarizing steps of injected current while tonic neurons fire repetitively. Based on microelectrode recordings from intact sympathetic ganglia, many investigators have concluded that virtually all paravertebral sympathetic neurons are phasic and that prevertebral sympathetic ganglia contain mixtures of phasic and tonic cells (Erulkar & Woodward, 1968; Weems & Szurszewski, 1978; Galvan & Sedlmeir, 1984; Cassell *et al.* 1986; Keast *et al.* 1993; Wang & McKinnon, 1995; Jobling & Gibbins, 1999; Janig, 2006). In the prevertebral inferior mesenteric ganglion (Cassell *et al.* 1986) it has been further suggested that phasic and tonic neurons may represent functional cell types, which in this example selectively control blood flow and visceral motility.

Despite the consistency of reports that paravertebral neurons are phasic when assessed in intact ganglia with sharp microelectrodes, a different picture emerges from studies in primary cell culture using whole cell patch clamp recordings. For example, comparing the excitability of identified secretomotor B neurons and vasomotor C neurons from dissociated bullfrog paravertebral sympathetic ganglia revealed that about one-quarter of the cells in both groups were slowly adapting or tonic, rather than phasic (Kullmann & Horn, 2010*b*). However, C cells were more easily excited than B neurons when stimulated with virtual nicotinic synapses synthesized by the dynamic clamp method. This suggests that phenotypic differences in excitability may exist, but are not necessarily linked to repetitive firing dynamics. Examples of tonic firing in mammalian SCG neurons are also evident in tissue culture studies of K^+ channel expression (Malin & Nerbonne, 2000, 2002) and nerve growth factor (NGF) signalling (Luther & Birren, 2006; Jia *et al.* 2008; Luther & Birren, 2009*a*,*b*). Together, these observations raise an important question. Are the differences in firing dynamics between studies of intact paravertebral ganglia and studies of dissociated ganglia due to the influence of cell culture conditions or are they a consequence of the difference between recordings with microelectrodes and patch electrodes? To answer this question, we performed whole cell recordings from acutely isolated intact ganglia to search for tonic cells that had not been observed in microelectrode experiments. We then used the dynamic clamp method to add a non-depolarizing shunt conductance to cells in culture and thereby mimic the damage associated with microelectrode recordings.

Another goal of the present work was to understand better *in vivo* intracellular recordings from mammalian sympathetic ganglia. Sympathetic neurons in paravertebral ganglia typically receive one strong nicotinic input that always triggers an action potential. We have proposed that the strength and convergence of weaker subthreshold inputs can result in additional action potentials and thereby generate gain by amplifying preganglionic activity (Karila & Horn, 2000; Horn & Kullmann, 2007). The gain hypothesis rests on the idea that summation between pairs of subthreshold EPSPs is sufficient to initiate action potentials in ganglion cells. Although support for the gain hypothesis comes from computational simulations, together with microelectrode recordings from isolated intact ganglia and dynamic clamp studies of bullfrog neurons (Karila & Horn, 2000; Wheeler

et al. 2004; Kullmann & Horn, 2006; Rimmer & Horn, 2010; Kullmann & Horn, 2010*a*), another critical test would be to analyse synaptic activity in living animals. Such experiments are extremely difficult and to date have yielded contradictory results. Pioneering intracellular microelectrode recordings from the rabbit and rat SCG indicated that subthreshold nicotinic EPSPs have little impact on the spike output of sympathetic neurons (Skok & Ivanov, 1983; McLachlan *et al.* 1997, 1998; McLachlan, 2003). However, more recent recordings from the rat third lumbar (L3) ganglion point to an important role played by weaker EPSPs (Bratton *et al.* 2010). By estimating the leak conductance associated with microelectrode damage, we sought to understand the consequences for estimates of synaptic gain.

Methods

The Institutional Animal Care and Use Committee at the University of Pittsburgh approved all animal protocols for this study. All experiments conform to the principles of UK regulation, as described in Drummond (2009).

Primary cell culture

Litters of postnatal day 12–15 Sprague–Dawley rat pups (CD strain; Charles River, Wilmington, MA, USA) were anaesthetized with isoflurane (Piramal Critical Care, Bethlehem, PA, USA) and killed by thoracotomy and cutting the heart. SCGs were then dissected, desheathed and cut into pieces before digestion. Pooled tissue was incubated (30 min, 37°C water bath) in 1–2 mg ml^{-1} collagenase 4 (CLS4; Worthington, Lakewood, NJ, USA) in L-15 medium with 2.05 mM glutamine (Hyclone SH30525.01; GE Healthcare Life Sciences, Logan, UT, USA). Then the collagenase solution was replaced with 0.25% trypsin in balanced saline (15050-57; Gibco, Grand Island, NY, USA) and the tissue further incubated for 30 min at 37°C. Digested SCGs were transferred to minimum essential medium (Richter's modification with L-glutamine, Hyclone SH30601.01) and triturated using three, fire polished Pasteur pipettes with graded tip sizes. Cells were spun down, resuspended in 400 μl of growth medium and plated on eight to twelve 12 mm round poly-D-lysine/laminin coated coverslips (354097; BD Biosciences, San Jose, CA, USA) in a 12 well plate. One hour after plating, 2 ml of additional growth medium was added to each well and the cells were returned to the 37°C, 5% CO_2 incubator. Growth medium contained minimum essential medium, 10% fetal bovine serum (Atlanta Biologicals, Norcross, GA, USA), 1% penicillin/streptomycin 10/10 solution (Atlanta Biologicals), 50 ng ml^{-1} NGF (BT5017; Harlan Bioproducts, Indianapolis, IN, USA) and 0.4–1 μM cytosine arabinoside hydrochloride (Sigma-Aldrich, St. Louis, MO, USA). Growth medium in cultures was replaced daily and recordings were made at room temperature (22°C), 2–6 days after plating.

Acute isolation of intact ganglia for whole cell patch recording

Adult male Sprague–Dawley rats (180–250 g, 6–8 weeks old, Charles River) were killed by CO_2 inhalation. The SCG with attached nerves was isolated, the connective tissue sheath was slit open and the ganglion then pinned out in a Sylgard-lined recording chamber. Throughout initial dissection, the SCG was continuously immersed in mammalian Ringer solution that contained (in mM): 146 NaCl, 4.7 KCl, 2.5 $CaCl_2$, 0.6 $MgSO_4$, 1.6 $NaHCO_3$, 0.13 NaH_2PO_4, 20 Hepes acid and 7.8 glucose (pH 7.3), gassed with 100% O_2. Tight fitting suction electrodes were then applied to the cervical sympathetic trunk for presynaptic stimulation and to the carotid nerves for postsynaptic extracellular recording (Li & Horn, 2006). After testing the preparation and electrodes by recording postganglionic compound synaptic responses, the Ringer solution was replaced by L15 medium with 2.05 mM glutamine, supplemented with 14 mM $NaHCO_3$ and 10 mg ml^{-1} collagenase 3 (CLS3, Worthington). The recording chamber was then placed for 1 h into a 37°C, 5% CO_2 tissue culture incubator (Hayar *et al.* 2008). The enzyme-treated preparation was then washed with mammalian Ringer solution and mounted on a fixed stage Zeiss Axioskop microscope equipped with a 40× water immersion objective and Nomarski DIC optics. During recording, the ganglion was superfused with Ringer solution at 2 ml min^{-1} using a peristaltic pump and maintained at 30°C by an inline heater (Warner Instruments, Hamden, CT, USA).

Electrophysiology of dissociated neurons

Whole cell patch recordings were made with heat-polished 2–4 MΩ pipettes fabricated from Schott 8250 glass (593600; A-M Systems, Sequim, WA, USA) using a P-87 puller (Sutter Instrument, Novato, CA, USA). The internal pipette solution contained (in mM): 94 potassium gluconate, 30 KCl, 10 phosphocreatine di(tris) salt, 10 Hepes, 0.2 EGTA, 4 Mg_2ATP, 0.3 Na_2GTP; pH 7.3.

Coverslips with cells were transferred to a recording chamber on a Zeiss IM35 inverted microscope and superfused at 1 ml min^{-1} with mammalian Ringer solution. From the composition of internal and external solutions, a junction potential of 14 mV was calculated using the utility in pClamp 10.3 (Molecular Devices, Sunnyvale, CA, USA).

This potential was compensated after placing the electrode in solution before patch formation. Recordings were made with an Axoclamp 2B amplifier (Molecular Devices) set to bridge current clamp mode and were filtered at 10 kHz. Data acquisition and dynamic clamp control at 20 kHz was implemented with G-clamp 2.2 software (Wheeler *et al.* 2004), which employs LabVIEW-RT and associated hardware (National Instruments, Austin, TX, USA). Cells included in the analysis were stable recordings (typically 1 h) with resting membrane potentials (V_{rest}) ≤ -60 mV and input resistance (R_{in}) ≥ 300 MΩ. Stability was judged by constant monitoring of the threshold synaptic conductance (thresh-g_{syn}), which is the minimum synaptic conductance needed to elicit an action potential (Wheeler *et al.* 2004).

Electrophysiology of intact ganglia

Patch pipettes used to record from the enzyme treated SCG were similar to those used in cell culture experiments and filled with the same internal solution. Only cells in which a giga-ohm seal was achieved before breaking the patch and entering whole cell recording mode were included in the analysis. A few cells showing spontaneous pacemaker activity similar to that seen in the pre-vertebral rabbit coeliac ganglion (Gola & Niel, 1993) were excluded from the present study. Current clamp recordings employed an Axoclamp 2B amplifier with filtering set to 10 kHz. Data were digitized at 10 kHz and stored with a Digidata 1440A interface and pClamp 10.3 (Molecular Devices).

Experimental protocols and analysis

Current–voltage (*I–V*) relationships were constructed from responses to families of 1 s current pulse injections. The membrane potential (V_m) during the last 10 ms of the response was taken as the steady-state voltage response. R_{in} was calculated from the slope of the *I–V* curve at V_{rest}. Frequency–current (*f–I*) relations were measured from the *I–V* data by calculating the instantaneous frequency between the last two spikes in each response. Ramp currents (0–400 pA over 5 s) and swept sinusoidal (ZAP) currents (0–50 Hz over 30 s) were generated using G-clamp.

Virtual nicotinic synaptic currents $I_{syn}(t)$ were implemented in dynamic clamp according to $I_{syn}(t) = g_{syn}(t)\ s\ (V_m - E_{rev})$ (Schobesberger *et al.* 2000). Based on synaptic currents measured in the rat SCG (Sacchi *et al.* 2006), synaptic conductance (g_{syn}) as a function of time (t) was modelled as the sum of two exponentials, with time constants of 1 ms for the rising phase and 7 ms for the decay phase. The synaptic reversal potential (E_{rev}) was set to 0 mV (Derkach *et al.* 1983). Synaptic strength at the peak of the conductance waveform was adjusted during experiments using a scaling factor (s). The strengths of virtual synapses in conductance templates were normalized to thresh-g_{syn} (Wheeler *et al.* 2004), but only after three or more consecutive measurements had established that thresh-g_{syn} was stable. Thresh-g_{syn} was found by an automated binary search routine that delivers virtual EPSPs of varying strength at 0.5 Hz and settles on a stable solution within 10 trials (Kullmann *et al.* 2004). Except where noted strong primary synapses were set to 300% thresh-g_{syn} and weak secondary synapses were set to 90% thresh-g_{syn}.

To create a non-depolarizing virtual leak conductance (g_{leak}) with dynamic clamp, g_{leak} was modelled as time invariant, with $E_{rev} = V_{rest}$. Anti-leak conductances were implemented by assigning a negative value to g_{leak} (Tucker *et al.* 2012).

For experiments to measure synaptic gain, dynamic clamp command templates were designed to model noisy baroreceptor-entrained synaptic activity. We assumed an average heart rate of 5 Hz (McLachlan *et al.* 1998), an average presynaptic firing rate (f_{pre}) of 1 Hz for each synapse (Ivanov & Purves, 1989; Ivanov, 1991) and a 20% on/off duty cycle for bursts of activity during each heartbeat (McAllen & Malpas, 1997). As in previous work and in the absence of evidence to the contrary, it was assumed that a common pool of preganglionic neurons forms primary and secondary nicotinic synapses in paravertebral ganglia (see fig. 8 in Karila & Horn, 2000). Convergence was modelled as one strong suprathreshold nicotinic synapse and eight weak subthreshold synapses (Purves *et al.* 1986; Karila & Horn, 2000). In this way, 40 s long synaptic templates containing 200 cardiac cycles were constructed at 50 μs resolution that permitted the dynamic clamp to operate at 20 kHz. For each 200 ms cardiac cycle, every synapse fired randomly at 5 Hz during the same 40 ms period and was silent for 160 ms. The method for calculating exponentially distributed random intervals between synaptic events during the active period was as previously described (Wheeler *et al.* 2004). Synaptic gain was calculated as the frequency of postsynaptic action potentials (f_{post}) divided by f_{pre} (Wheeler *et al.* 2004). A gain >1 signifies that the population of postganglionic sympathetic neurons is firing faster than the population of preganglionic neurons that drives it (Karila & Horn, 2000).

Data were analysed and figures prepared using Igor (v6.2; Wavemetrics, Lake Oswego, OR, US) and Excel. Grouped data are expressed as the mean ± SEM. Statistical comparisons were made, as appropriate, using an ANOVA and Tukey *post-hoc* test or *t* tests, with $P < 0.05$ as the criterion for significance (Prism; GraphPad, LaJolla, CA, USA).

Results

Dissociated superior cervical ganglion neurons exhibit three classes of excitability

To assess firing dynamics, *I–V* relations were constructed by stimulating SCG neurons with families of 1 s, 30 pA current steps ranging in amplitude from −240 to +240 pA (Fig. 1). As in previous cell culture studies, the phasic-tonic dichotomy failed to capture the full scope of responses because some cells displayed an intermediate behaviour (Malin & Nerbonne, 2000, 2002; Luther & Birren, 2006; Jia *et al.* 2008; Luther & Birren, 2009*b*). The data were better described using Hodgkin's criteria for class 1, class 2 and class 3 excitability (Hodgkin, 1948; Rinzel &

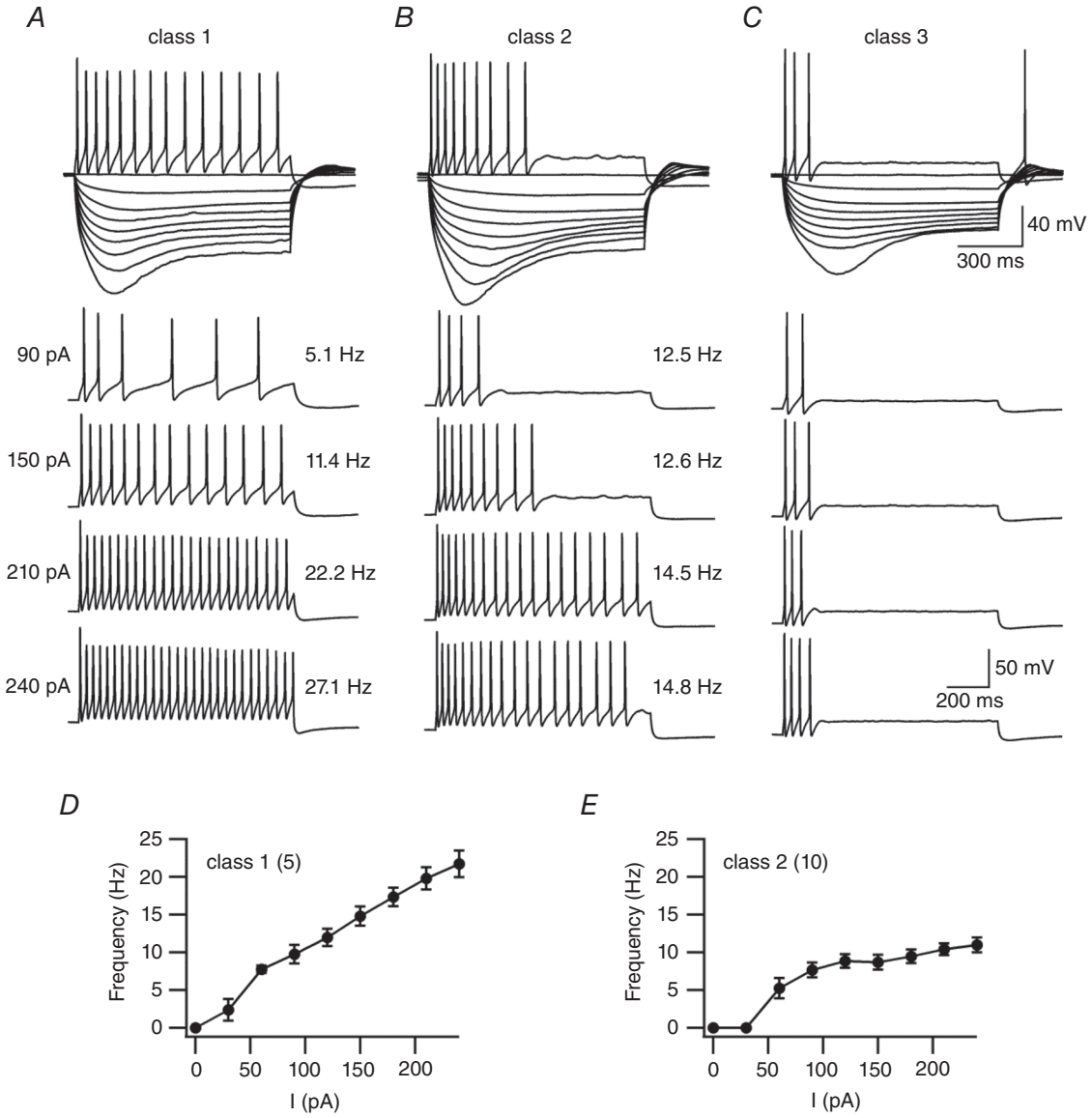

Figure 1. Three types of firing dynamics in dissociated superior cervical ganglion neurons
A–C, examples of current–voltage relations recorded by stimulating neurons with families of 1 s, 30 pA steps ranging from −240 to 240 pA. *A*, class 1 neurons fired repetitively at frequencies that increased in proportion to the depolarizing current strength. *B*, class 2 neurons also fired repetitively, but adapted and ceased firing at lower stimulus strengths. In class 2, firing frequency remained relatively constant over the range of responses. *C*, class 3 neurons fired a brief phasic burst of one to four spikes. Average frequency–current relationships distinguished between groups of class 1 (*D*) and class 2 (*E*) neurons. Numbers in parentheses denote the size of each group. *D*, action potential frequency in class 1 neurons increased linearly with current injection strength. *E*, transition between quiescence and firing in class 2 neurons was more abrupt than in class 1 neurons and the frequency–current slope was more shallow. All firing rates were calculated as the instantaneous frequency for the last two spikes in each response.

Ermentrout, 1989; Izhikevich, 2007; Prescott *et al.* 2008*a*). In ideal responses to depolarizing current steps derived from the analysis of mathematical models, class 1 neurons fire repetitively at arbitrarily low rates that increase in proportion to stimulus strength, class 2 neurons also fire repetitively, but in a narrow band of frequencies regardless of stimulus strength, and class 3 neurons only fire once.

Figure 1*A* illustrates a neuron where tonic class 1 firing occurred throughout the duration of depolarizing steps at rates that were smoothly graded from 5.1 Hz to 27.1 Hz. Figure 1*B* illustrates a class 2 neuron where firing ceased before the end of lower amplitude current pulses, but persisted for the entire 1 s duration of stronger stimuli. As is typical of class 2 dynamics the firing rate varied narrowly in this example between 12.5 and 14.8 Hz. A third behaviour was seen in phasic class 3 neurons, which fired two to four spikes at most, even with the strongest stimuli (Fig. 1*C*). In a sample of 28 neurons, five cells (18%) displayed tonic class 1 excitability, 10 cells (36%) displayed class 2 excitability and 13 cells (46%) displayed phasic class 3 excitability. The distinction between class 1 and class 2 neurons was readily discerned in *f–I* curves constructed for individual cells and with grouped data. The slope of the *f–I* relation was relatively steep for class 1 cells, where *f* varied over a 9.4-fold range (Fig. 1*D*) and relatively flat for class 2 cells, where *f* varied over a 2.1-fold range (Fig. 1*E*). R_{in} tended to be lower in class 3 neurons (413 ± 19 MΩ, $n = 13$) than in class 1 (474 ± 54 MΩ, $n = 5$) or class 2 neurons (496 ± 26 MΩ, $n = 10$), but the differences were not significant. Similarly, class 1, class 2 and class 3 cells did not differ in terms of their V_{rest} (-65 ± 1.0 mV; -71 ± 1.7 mV; -67 ± 1.1 mV) or membrane time constants (τ) (39 ± 3.2 ms; 39 ± 2.2 ms; 38 ± 1.7 ms).

Stimulating neurons with current ramps, rather than steps, also proved effective for distinguishing between the three classes of excitability (Fig. 2*A*). The minimum step for evoking spikes (i.e. rheobase) in these experiments was generally between 30 and 90 pA (Fig. 1). We therefore employed 5 s ramps whose final value was 400 pA, which is far larger than the rheobase. Class 1 neurons ($n = 5$) began firing very close to the beginning of the ramp at rates that gradually increased throughout the ramp. Class 2 neurons ($n = 5$) eventually fired repetitively, but only towards the end of the ramp and class 3 neurons ($n = 4$) did not fire at all in response to the 400 pA ramp stimuli.

A large depolarizing sag was prominent during hyperpolarizing responses to current steps in all three classes of neurons (Figs 1, 3, 6 and 7). The sag is attributable to inward h-type cation current because it is activated at negative potentials and blocked by ZD7288, a selective h-channel antagonist (data not shown). This confirms previous reports of h-current in mouse and rat SCG neurons (Lamas, 1998; Jobling & Gibbins, 1999). Currents through h-channels are of possible interest because they may influence V_{rest}, synaptic integration and subthreshold oscillations of V_m (Izhikevich, 2007).

Indeed subthreshold oscillations of V_m were sometimes evident during ramp stimuli. Examples can be seen in Fig. 2*A* just before firing by the class 1 cell and midway during the ramp in the class 2 cell (downward arrow). This might signify membrane resonance, which could be an important factor leading to supra-linear temporal summation between subthreshold nicotinic EPSPs (Izhikevich, 2007). To test for resonance, neurons were stimulated with ZAP stimuli whose sinusoidal frequency increased linearly from 0 to 50 Hz over 30 s and whose amplitude ranged from +20 pA to −20 pA (Fig. 2*B*). Using this approach, we did not detect resonance in five class 1 cells, five class 2 cells and six class 3 cells. Instead, the membrane voltage response decreased monotonically with the increasing frequency of sinusoidal stimulation (Fig. 2*B*).

Class 1 and class 2 excitability in the intact superior cervical ganglion

The observation that the majority of SCG neurons in tissue culture display class 1 or class 2 excitability strongly contradicts the intact ganglion literature (*cf.* Introduction), which states that 95–100% of SCG neurons exhibit class 3 excitability (Wang & McKinnon, 1995; Jobling & Gibbins, 1999). One explanation for this striking disparity is that growing dissociated neurons for several days in the presence of serum and NGF transforms them into an unnatural state. To test this possibility, we circumvented tissue culture by implementing a method for whole cell patch recording in the acutely isolated intact SCG. Surprisingly, class 3 neurons were undetectable in SCG patch recordings when a giga-ohm seal was formed before rupturing the on-cell patch. In a series of 28 cells meeting this criterion, 20 (71%) displayed class 1 excitability (Fig. 3*A*) and eight cells (29%) displayed class 2 excitability (Fig. 3*B*). In cells where the on-cell patch ruptured before achieving a giga-ohm seal, R_{in} was <100 MΩ and firing was class 3. We interpreted the low R_{in} as evidence of improper seal formation (i.e. damage) and excluded these cells from further analysis.

The slope of the *f–I* relation in class 1 neurons from intact ganglia (Fig. 3*C*) was less steep than seen in cultured neurons (Fig. 1*D*). One explanation is that neurons in the intact ganglion were exquisitely sensitive, often firing in response to 10 pA current pulses and at lower frequencies than seen in cell culture. None the less, the class 2 neurons displayed a distinctive abrupt transition from quiescence to firing, which required a larger current (40 pA) than needed to evoke firing in class 1 cells and whose rate was quite invariant over the range of currents tested (Fig. 3*D*). Comparing the passive membrane properties revealed that

the average V_{rest} of class 1 neurons was 5 mV depolarized to that of class 2 neurons (Fig. 3*E*, -59 ± 1.2 mV, -64 ± 1.4 mV, $P < 0.02$), but that the R_{in} of both groups did not differ (Fig. 3*F*) and was >500 MΩ.

Primary and secondary nicotinic EPSPs in the intact superior cervical ganglion

Occasional spontaneous nicotinic EPSPs were observed during measurement of *I–V* relations. Two examples in Fig. 3*A* (see upward arrows) have time courses >100 ms, which is much longer than generally recorded with microelectrodes (Skok & Ivanov, 1983; McLachlan *et al.* 1997; Bratton *et al.* 2010; Rimmer & Horn, 2010). To obtain a fuller picture, we also measured EPSPs evoked by graded presynaptic stimulation of the cervical sympathetic trunk. Figure 4 illustrates a cell where recruitment of presynaptic fibres was monitored by extracellular recording from the postsynaptic external carotid nerve, while a simultaneous intracellular patch electrode recording revealed EPSPs of increasing magnitude. In this example 50–60 μA shocks evoked subthreshold EPSPs that fluctuated in amplitude, 70 μA shocks evoked EPSPs that straddled threshold, and 80 μA shocks evoked strong suprathreshold responses. Strong suprathreshold EPSPs and weak subthreshold EPSPS such as these have been described as primary and secondary EPSPs (Karila & Horn, 2000). Finding that even the weakest EPSPs can last for hundreds of milliseconds supports the possibility that secondary EPSPs may summate at the very low rates of physiological activity seen in the intact sympathetic system of living animals and human subjects (Ivanov & Purves, 1989; Macefield *et al.* 1994; Janig, 2006).

Probing cellular excitability with virtual nicotinic synapses and leak channels

Having found that neurons in the acutely isolated intact ganglion express class 1 and class 2 firing dynamics, we hypothesized that the damage produced either by poor seal formation with patch electrodes or by microelectrode impalement results in a leak that profoundly alters cellular

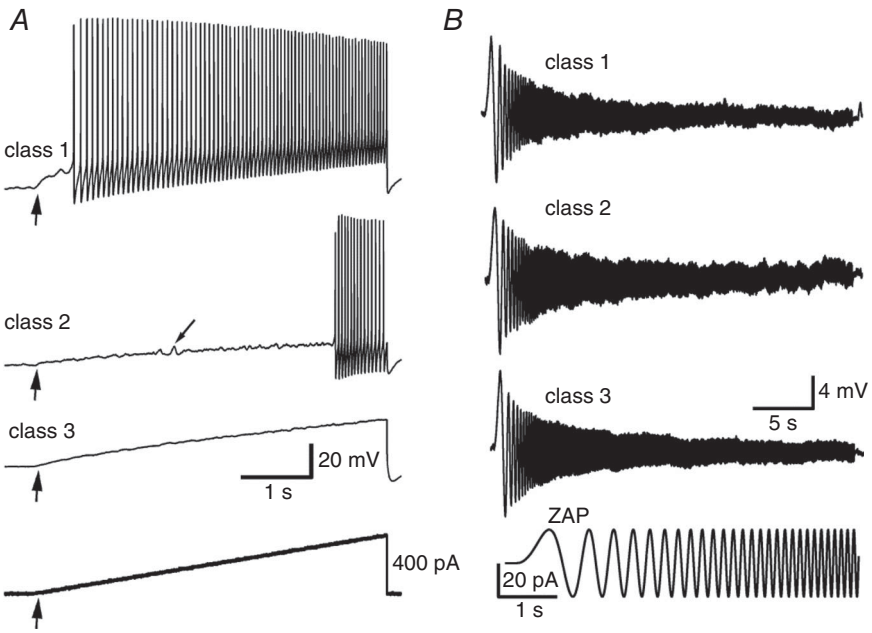

Figure 2. Responses of dissociated superior cervical ganglion neurons to current ramps and sinusoidal ZAP currents
A, responses to a depolarizing current ramp (5 s, 400 pA) (bottom trace), distinguished between class 1, 2 and 3 neurons that had been initially classified by frequency–current curves. The top trace illustrates a class 1 neuron that fired at a gradually increasing rate throughout most of the ramp. The second trace shows a class 2 neuron that fired only towards the end of the ramp. Downward arrow points to a spontaneous oscillation of membrane potential midway through this ramp response. The third trace shows a representative class 3 neuron that did not fire at all during the ramp. Upward arrows mark the start of each ramp. *B*, top three traces illustrate examples of responses in class 1, 2 and 3 neurons to a ZAP current (bottom trace), which was designed to detect resonance. The frequency of the sinusoidal ZAP current increased linearly from 0 to 50 Hz in 30 s. For clarity only the first 6 s of the ZAP current are shown. Cells displaying all three classes of firing dynamics responded similarly to the ZAP. The amplitude of the V_m sinusoids decreased smoothly as the stimulus frequency increased indicating an absence of resonance. ZAP, swept sine wave.

excitability and synaptic integration. To test this idea we returned to the cell culture model, where with the dynamic clamp we could implement virtual nicotinic EPSPs of defined strength and timing, together with virtual leak channels that would simulate the shunting associated with electrode damage.

Thresh-g_{syn} defines cellular excitability in terms of the minimum synaptic conductance required for V_m to reach spike threshold. Figure 5*A* illustrates a family of virtual EPSPs produced in an automated trial to find thresh-g_{syn} in a class 2 neuron. During the trial, g_{syn} was systematically increased when the V_m response was subthreshold and decreased when the V_m response was suprathreshold, until the stimulus settled at thresh-g_{syn} (Kullmann *et al.* 2004). Figure 5*A* also shows that the virtual EPSPs generated with dynamic clamp lasted >100 ms and were indistinguishable from the physiological EPSPs recorded from the intact ganglion (Fig. 4) with patch electrodes.

Thresh-g_{syn} was lowest in class 1 cells and highest in class 3 cells (Fig. 5*B*). On average, thresh-g_{syn} in class 3 neurons (4.60 ± 0.36 nS, $n = 13$) was significantly higher than in class 1 (2.52 ± 0.25 nS, $n = 5$, $P < 0.01$, ANOVA) and class 2 (3.08 ± 0.37 nS, $n = 10$, $P < 0.05$, ANOVA) neurons. To account for possible differences in cell size, whole cell capacitance (C_m) was calculated by dividing τ by R_{in}. Values for τ were obtained by fitting voltage transients during hyperpolarizing responses to small currents (30–60 pA) to a single exponential. When normalized to C_m, threshold-g_{syn} remained significantly higher in class 3 cells than in class 1 cells (Fig. 5*C*).

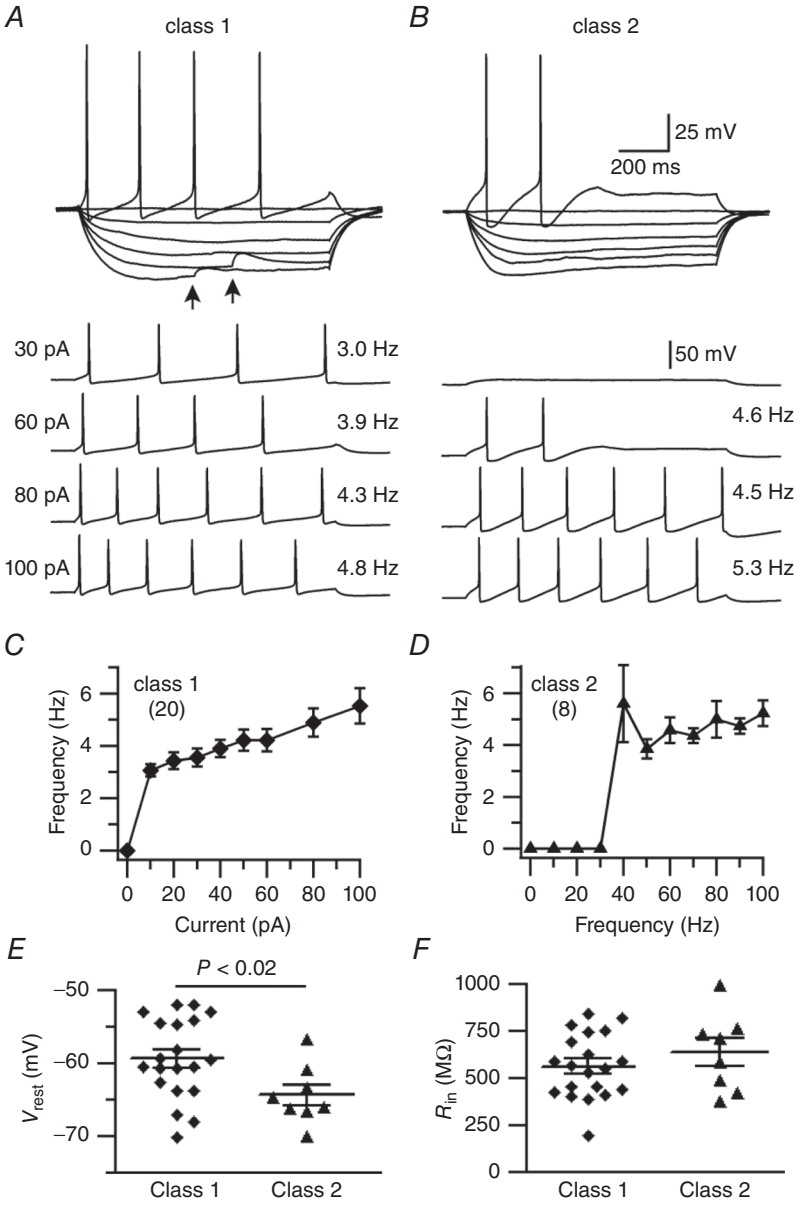

Figure 3. Whole cell recording from the intact superior cervical ganglion reveals neurons with class 1 and class 2 firing dynamics
A, example of a current–voltage relation from a sympathetic neuron with class 1 firing dynamics. Upward arrows point to spontaneous nicotinic EPSPs. The firing rate of this cell was smoothly graded over the range of currents tested. *B*, example of current–voltage relation from a cell with class 2 firing dynamics. Unlike the cell in (*A*), this cell did not fire in response to a 30 pA current pulse and adapted in response to the 60 pA stimulus. *C*, plot of the frequency–current relation for 20 neurons with class 1 firing dynamics. Note that this group of cells fired in response to 10 pA stimuli. *D*, plot of the frequency–current relation for eight neurons with class 2 firing dynamics. In these cells, the current threshold for firing was 40 pA, firing adapted during responses to weaker stimuli and the firing rate was more insensitive to the current strength than in class 1 cells. *E*, average V_{rest} of class 1 neurons was significantly less than in cells with class 2 firing dynamics, but the range for individual cells overlapped. *F*, average R_{in} was indistinguishable in neurons with class 1 and class 2 firing dynamics. Note that many of the cells in both groups had R_{in} in the range 500 MΩ–1 GΩ.

Table 1. Effects of a virtual leak conductance upon the passive membrane properties of sympathetic neurons

	Virtual g_{leak} (nS)			
Passive membrane properties	0	3 nS	10 nS	20 nS
V_{rest} (mV)	−68 ± 0.9	−68 ± 0.9	−68 ± 0.8	−68 ± 0.8
R_{in} (MΩ)	454 ± 17	182 ± 5	81 ± 1	44 ± 1
τ (ms)	38 ± 1.2	16 ± 0.6	6 ± 0.4	3 ± 0.3

Adding a non-depolarizing leak of 3–20 nS had no effect upon V_{rest} of dissociated superior cervical ganglion neurons, but produced significant reductions of R_{in} and τ at all levels (ANOVA). $n = 27$ cells for 20 nS g_{leak} and 28 cells for all other columns. Passive properties of class 1, 2 and 3 neurons were indistinguishable and therefore combined.

We next examined how virtual leak conductances alter the firing dynamics of sympathetic neurons. To create a non-depolarizing leak that would dissociate the effects of shunting from those of depolarization (e.g. Na^+ channel inactivation), the leak reversal potential (E_{leak}) was set to V_{rest}. Figure 6*A* illustrates a neuron with class 1 firing dynamics whose spike output and membrane resistance were reduced after adding 3 nS of g_{leak}. Increasing g_{leak} to 10 nS converted the cell to unambiguous phasic class 3 firing and a further increase to 20 nS g_{leak} made the cell inexcitable, all without changing V_{rest} (Table 1). Similar transitions were seen in the class 2 neuron illustrated in Fig. 6*B*. Adding 3–20 nS of g_{leak} converted this neuron to class 3 dynamics and then rendered it inexcitable. Every class 1 neuron ($n = 5$) and class 2 neuron ($n = 10$) was similarly converted to class 3 firing dynamics. Plots of steady-state *I–V* relations (Fig. 6*C*) showed that shunts of increasing magnitude caused a counter-clockwise rotation of the *I–V* relation around V_{rest}, combined with linearization as the shunt came to dominate total membrane conductance. Both effects are predicted by computational simulations of a simplified model sympathetic neuron (Schobesberger *et al.* 2000). The shunts also obscured sag responses caused by h-current. This implies that h-currents are much smaller than current through the virtual g_{leak} and explains why sag responses have rarely been reported in the SCG microelectrode literature (Jobling & Gibbins, 1999). As would also be expected, adding g_{leak} caused profound reductions in τ and R_{in} (Fig. 6*D* and *E*, Table 1). Based on reports that R_{in} ranges from 50 to 200 MΩ (Adams & Harper, 1995; McLachlan *et al.* 1997, 1998; Bratton *et al.* 2010; Springer, 2013), we estimate that microelectrode recordings introduce shunts of 3–18 nS.

Enhancement of repetitive firing by anti-leak channels

The trend towards lower R_{in} in dissociated class 3 neurons, though not significant, suggests the possibility that either

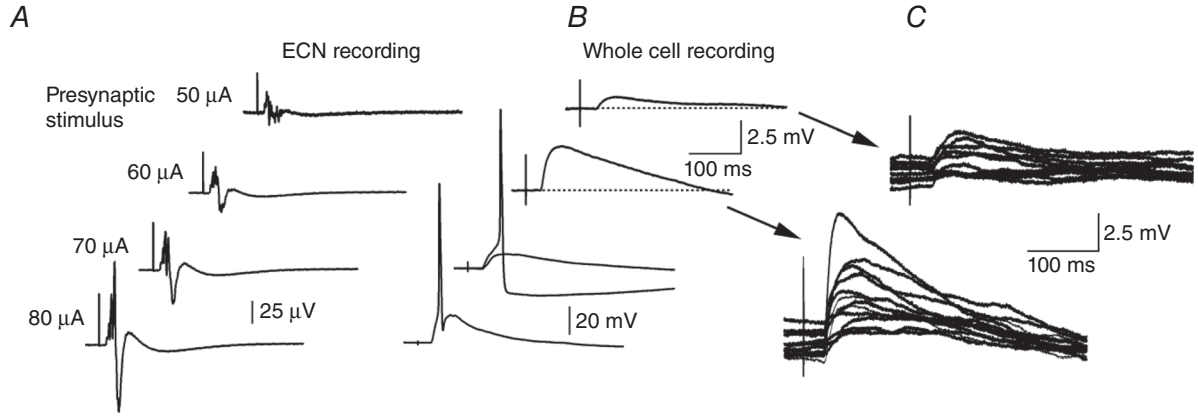

Figure 4. Recruitment of nicotinic EPSPs in the intact superior cervical ganglion using graded presynaptic stimuli
An example of simultaneous extracellular and intracellular recordings from the acutely isolated intact SCG. *A*, compound postsynaptic responses were recorded from the ECN. As stronger presynaptic stimuli were applied to the cervical sympathetic trunk, the compound responses grew larger in magnitude. *B*, simultaneous whole cell recordings from a class 1 SCG neuron. *C*, the subthreshold responses at the two lower stimulus intensities in panel *B* are averages comprised of the individual subthreshold secondary EPSPs shown here. In this experiment the postsynaptic responses evoked by 70 μA shocks straddled the action potential threshold. Increasing the stimulus to 80 μA recruited a suprathreshold primary EPSP that distorted the hyperpolarizing spike afterpotential to produce an early depolarizing component. ECN. external carotid nerve.

physiological variations in leak conductance or damage caused by a less than perfect seal in a patch recording may have been sufficient to influence the firing dynamics of some cells. To test this hypothesis, we introduced virtual anti-channels that would negate the intrinsic leak. Anti-channels behave like the normal channels generated by dynamic clamp, except that current flows in the opposite direction (Tucker *et al.* 2012).

Leak conductances were subtracted from class 2 ($n = 13$) and class 3 neurons ($n = 16$). Figure 7*A* illustrates a class 2 cell that was converted to class 1 dynamics (Fig. 7*B*) after subtracting a 2 nS g_{leak} with $E_{leak} = V_{rest}$. The associated *f–I* relations shifted as would be expected for the two firing profiles (Fig. 7*C*). In another cell that initially displayed class 3 dynamics (Fig. 7*D*), subtracting a 2 nS leak converted it to class 2 dynamics (Fig. 7*E* and *F*). However, not all cells could be transformed in this manner. Figure 7*G* illustrates a cell whose class 3 firing dynamics remained unchanged when virtual leaks of −2, −4 and −6 nS were applied. In all, we found that anti-leaks converted eight class 3 neurons to class 2, but none to class 1, and that anti-leaks had no effect on firing dynamics of eight other class 3 neurons. We also observed two class 2 neurons that were converted to class 1 by anti-leaks and 11 class 2 neurons that were impervious to anti-leaks. These observations show that variation in the magnitude of g_{leak}, whether natural in origin or created by recording damage, may account for some, but not all, of the diversity of firing dynamics seen in sympathetic neurons.

Shunting inhibition introduced by virtual leaks

Introduction of a virtual g_{leak} that does not change V_{rest} (Table 1) should produce pure shunting inhibition and thereby weaken nicotinic EPSPs. However, the

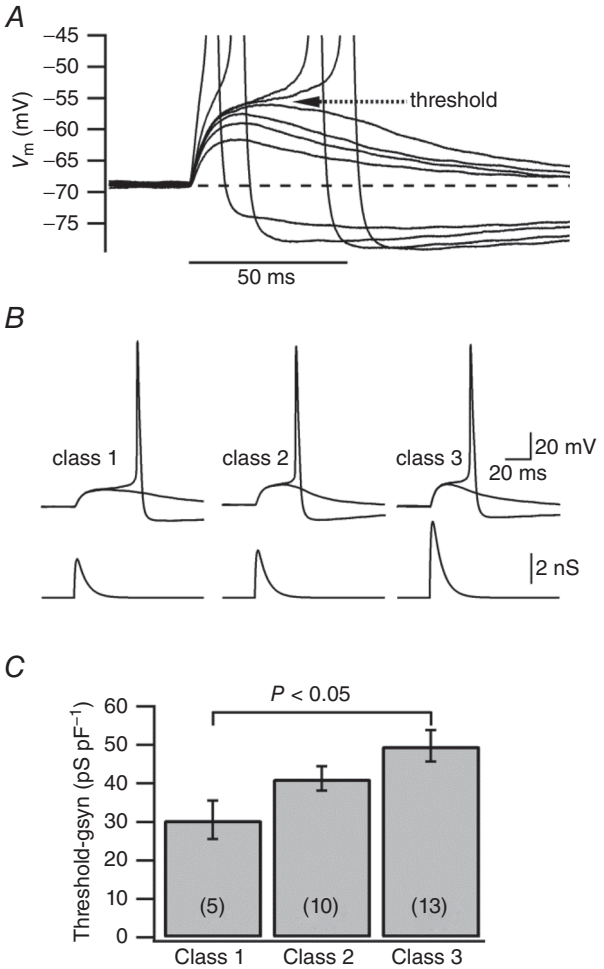

Figure 5. Threshold-g_{syn} (thresh-g_{syn}) is greatest in dissociated class 3 superior cervical ganglion neurons
A, postsynaptic responses evoked by a family of virtual nicotinic EPSPs during measurement of thresh-g_{syn} in a superior cervical ganglion neuron with class 2 firing dynamics. The three smallest virtual EPSPs have waveforms similar to the evoked EPSPs in Fig. 4. *B*, examples of thresh-g_{syn} in neurons with the three classes of firing dynamics. Upper traces show pairs of responses straddling spike threshold. Lower traces illustrate the underlying thresh-g_{syn}. *C*, thresh-g_{syn} normalized to cell size was significantly greater in class 3 cells than class 1 cells. Number of cells in each group in parentheses.

magnitude of such effects is uncertain. To determine the balance between physiologically relevant levels of synaptic excitation and realistic levels of inhibitory leak conductances, neurons were stimulated by a series of virtual nicotinic EPSPs whose strength was varied from 90% to 650% thresh-g_{syn} (Fig. 8). Subsequent introduction of a 3 nS g_{leak}, which corresponds to a high-quality microelectrode recording, was sufficient to increase the synaptic conductance needed to reach threshold. This effect became larger when g_{leak} was increased to 10 nS and then 20 nS. We observed the same behaviour in 19 neurons whose initial firing dynamics belonged to class 1 ($n = 3$), class 2 ($n = 7$) and class 3 ($n = 9$). These results imply that regardless of firing dynamics, introduction of a shunt

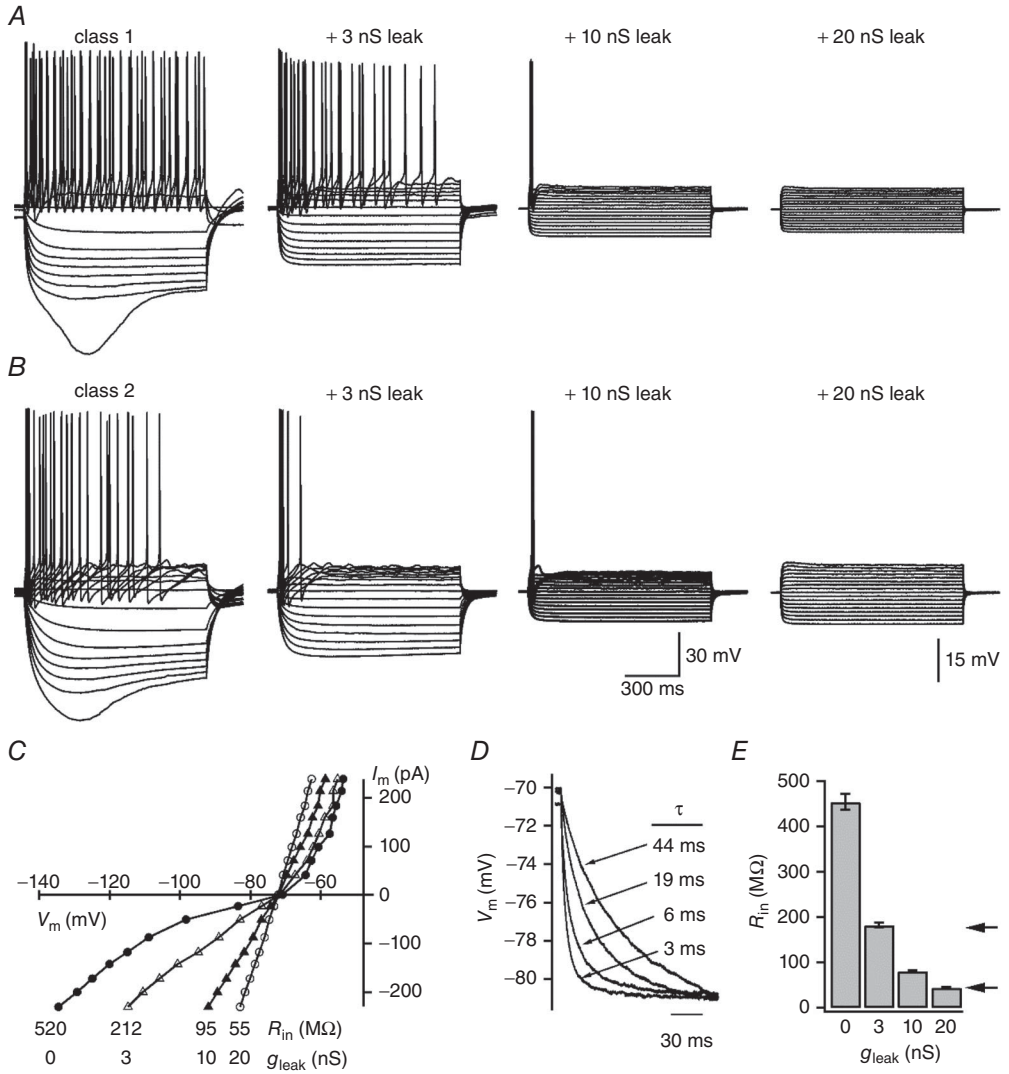

Figure 6. Virtual leak channels shift firing dynamics from classes 1 and 2 to class 3
A and *B*, examples of a dissociated class 1 superior cervical ganglion (SCG) neuron and a class 2 SCG neuron, before and after addition of a non-depolarizing leak (g_{leak}) produced by setting E_{rev} equal to V_{rest} under dynamic clamp. Calibrations of records for both neurons are the same. Adding a 3–10 nS g_{leak} shifted both neurons to class 3 phasic firing and 20 nS g_{leak} made both cells inexcitable over the range of currents tested. In each panel, the neuron was stimulated with a family of 1 s, 30 pA current steps. *C*, steady-state current–voltage plots for the records in (*B*) illustrate the linearization and rotation around V_{rest} produced by g_{leak}. The corresponding reductions of R_{in} are noted below the graph. *D*, addition of g_{leak} also produced a progressive decrease in the time constants for membrane hyperpolarization. Traces of similar amplitude from the four current–voltage relations in (*B*) were superimposed and fit to single exponentials. The slowest τ (44 ms) was observed in the unperturbed cell and the fastest τ (3 ms) was after addition of a 20 nS g_{leak}. *E*, grouped data show how virtual leaks systematically reduced R_{in} (28 neurons representing all three classes of excitability). Arrows on right mark the range of R_{in} commonly observed in microelectrode recordings from neurons in the intact SCG and in other autonomic ganglia (Adams & Harper, 1995).

conductance similar in magnitude to that associated with microelectrode recording was sufficient to weaken the impact of secondary nicotinic synapses and probably reduces the synaptic gain resulting from summation of secondary EPSPs. It also indicates that the ability of primary EPSPs to initiate action potentials is impervious to all but the most extreme microelectrode damage.

Phase plane trajectories of action potentials driven by virtual and physiological synapses

The interplay between synaptic and non-synaptic currents provides another means for examining how strong and weak EPSPs drive action potentials and how this interaction may change in the face of shunts. For this purpose, we constructed phase plane plots of dV_m/dt as a function of V_m (Fig. 9). The first derivative of V_m is proportional to the sum of all ionic currents flowing across the cell membrane at a given instant in time. Phase plane plots therefore reflect the total membrane current flowing at each membrane potential during action potential cycles driven by synaptic stimulation in cell culture (Fig. 9*A*) and in the intact SCG (Fig. 9*C*). For convenience, the cycle was divided into phases of excitation, activation and recovery (Fig. 9*A*, control). Phase 1 begins with V_m at rest, where $dV_m/dt = 0$ V s^{-1}, and proceeds through the EPSP and spike threshold. Phase 2 corresponds to the action potential upstroke, includes the overshoot and ends at the peak of the spike. Phase 3 begins with membrane repolarization followed by the spike afterhyperpolarization (AHP) and ends with the membrane returning to the original stable V_{rest}.

The results in Fig. 9*A* were representative of 19 dissociated neurons studied in the absence and presence of virtual leaks. We saw no difference in the appearance of phase plane plots of action potentials from cells belonging to class 1 ($n = 3$), class 2 ($n = 7$) and class 3 ($n = 9$). In this and subsequent analysis of EPSPs in the intact ganglion (Fig. 9*A* and *B*), the peak currents through voltage-gated channels dwarfed all synaptic currents. Peak dV_m/dt during virtual and physiological EPSPs never exceeded 25 V s^{-1}, while peak dV_m/dt was always in the range 125–250 V s^{-1} during action potentials.

The family of phase plane trajectories in Fig. 9*A* was constructed for action potentials driven by virtual EPSPs

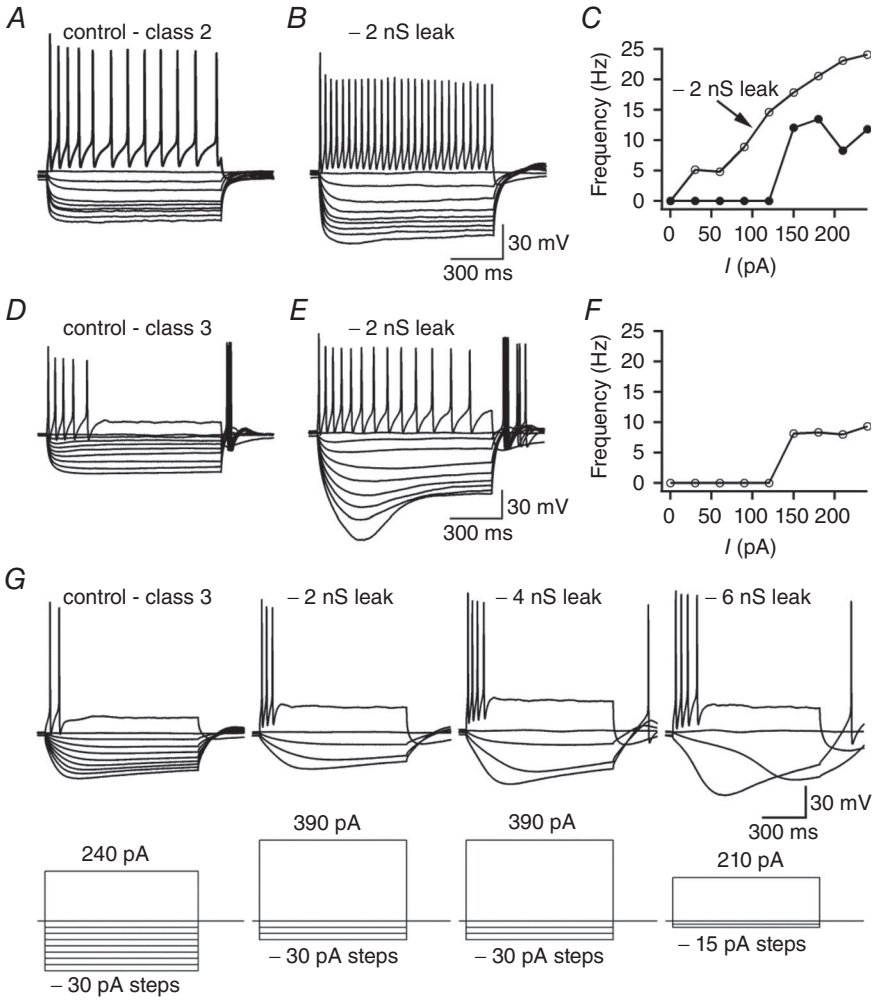

Figure 7. Anti-leak conductances shift firing dynamics away from class 3 in some, but not all, dissociated superior cervical ganglion neurons
A, current–voltage relation of a class 2 neuron stimulated with 1 s, 30 pA current pulses. *B*, after subtracting a 2 nS non-depolarizing g_{leak} the firing rate during depolarization increased in a graded fashion. This was accompanied by an increase in membrane resistance evident from the larger amplitude shifts in membrane potential during injection of hyperpolarizing current steps. *C*, frequency–current relations show that the anti-g_{leak} shifted this cell from class 2 to class 1 firing dynamics. *D*, example of a cell in which firing dynamics were initially class 3. *E*, after subtracting 2 nS g_{leak}, this cell fired repetitively and membrane resistance increased. *F*, frequency–current relation with the anti-g_{leak} shows the narrow range of firing frequencies that identify the dynamics as class 2. *G*, example of a cell whose class 3 firing dynamics remained unchanged even with progressive subtraction of 2, 4 and 6 nS g_{leak}. Lower panels illustrate the current pulses used for each current–voltage relation. Although a striking increase in membrane resistance was evident during the anti-leak, there was no shift away from phasic firing in this neuron.

of defined strength using the data in Fig. 8. V_{rest} in this cell was about −65 mV under control conditions and in the presence of the virtual g_{leak}. During phase 1 of the cycle under control conditions one can see the family of synaptic currents evoked by a virtual synapse whose strength was varied from 100 to 650% thresh-g_{syn}. During phase 2, the region of V_m where dV_m/dt began to increase precipitously was seen to vary with the magnitude of g_{syn}. In particular, the apparent threshold for the response to a 100% thresh-g_{syn} stimulus was hyperpolarized to responses for stronger stimuli. In addition the peak inward current (maximum dV_m/dt), which occurred during phase 2, was lower for spikes driven by weaker synaptic conductances. Both of these effects can be understood by considering the voltage trajectories of spikes during measurements of thresh-g_{syn}, as illustrated in Fig. 5*A*. When g_{syn} is very close to threshold in strength one can see that the active response develops slowly near the peak of the EPSP. This contrasts to action potentials triggered by stronger EPSPs, which reach threshold tens of milliseconds earlier at the beginning of the EPSP. With stronger EPSPs, the first sign of an active response appears as an inflection in the voltage trajectory at more positive potentials than active responses to weaker EPSPs. The difference in time to threshold also suggests an explanation for the reduced peak inward current during the spike driven by the 100% thresh-g_{syn} stimulus. Peak dV_m/dt occurs when V_m is close to 0 mV. Because the reversal potential for the virtual synaptic currents was set to 0 mV, this implies that almost all current flow at peak dV_m/dt is through non-synaptic voltage-gated Na^+ channels. Depolarization during the delayed onset of spikes driven by weaker EPSPs (Fig. 5*A*) therefore probably causes partial inactivation of the voltage-dependent Na^+ conductance, resulting in smaller inward currents. Finally, the strength of EPSPs also influenced phase plane trajectories during the AHP at the end of phase 3. The weakest EPSPs produced the smallest distortion of AHPs and the most negative values for V_m (Fig. 9*B*).

Although g_{leak} reduced the excitatory strength of virtual EPSPs (Fig. 8), it had very little effect on the general shape of phase plane trajectories (Fig. 9*A*). However, closer inspection reveals that with 3 nS and 20 nS g_{leak} there was a systematic reduction of peak dV_m/dt during phase 2 (upstroke). Under these conditions, the inward current through voltage-gated Na^+ channels at peak dV_m/dt was reduced by outward current through g_{leak}. The relatively small magnitude of the reduction in total current produced by g_{leak} indicates that the leak currents were much smaller than the voltage-gated Na^+ current.

In parallel experiments, phase plane plots of spikes from neurons in the acutely isolated intact SCG strongly resembled those constructed from cell culture recordings. In four neurons, we compared phase plane plots of spikes

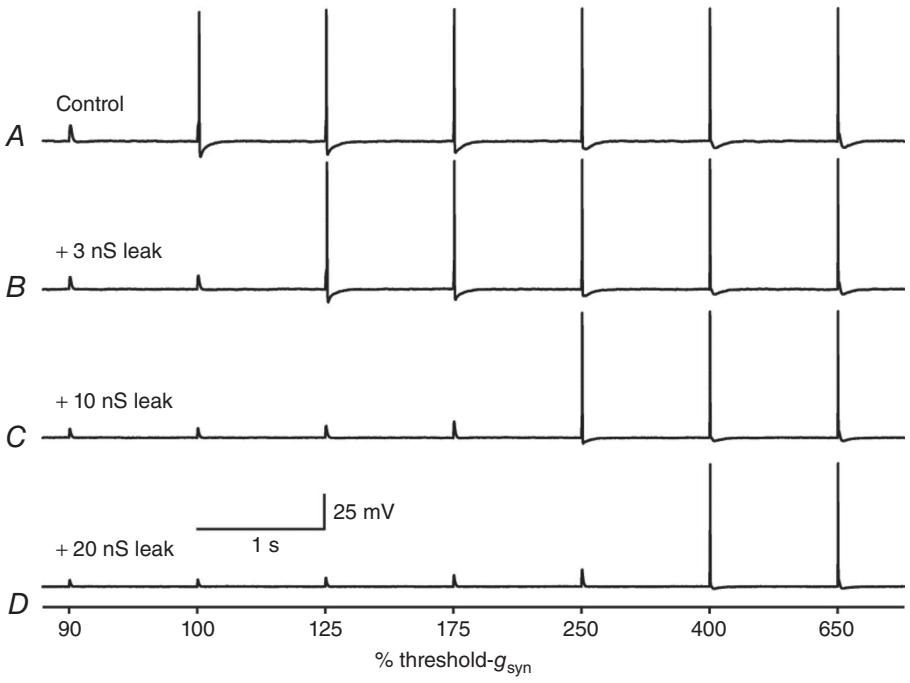

Figure 8. The balance between g_{leak} and the efficacy of virtual nicotinic EPSPs
A, family of EPSPs elicited by virtual synaptic conductances of increasing strength (90–650% threshold-g_{syn}) in a dissociated superior cervical ganglion neuron. *B–D*, the same virtual EPSPs were elicited after addition of 3, 10 and 20 nS g_{leak}. This resulted in a systematic reduction in the efficacy of EPSPs. In the face of the non-depolarizing leaks, it took more g_{syn} to trigger an action potential.

that were triggered by secondary (weak) EPSPs and by primary (strong) EPSPs evoked with graded presynaptic stimuli (e.g. Fig. 4). Figure 9*B* illustrates an example of several action potentials triggered by EPSPs that were very close to threshold in strength (grey) and other spikes triggered by much stronger EPSPs (black). The phase plane plot of these responses (Fig. 9C) showed that once again the currents attributable to voltage-gated channels are much larger than the synaptic currents. Differences in dV_m/dt between strong and weak EPSPs are clearly visible near the origin of the cycle, yet somewhat subtle in comparison to peak dV_m/dt during the action potential. Another notable feature is the large AHP that is most prominent in spikes driven by weaker EPSPs. The AHP shifted dV_m/dt to more negative V_m during the final part of phase 3, but to a lesser degree when strong EPSPs deformed it to produce an afterdepolarization.

In a recent study of living animals, phase plane trajectories of intracellular microelectrode recordings from the L3 sympathetic ganglion were used as one criterion for distinguishing action potentials driven by naturally occurring strong and weak EPSPs (Fig. 5 in

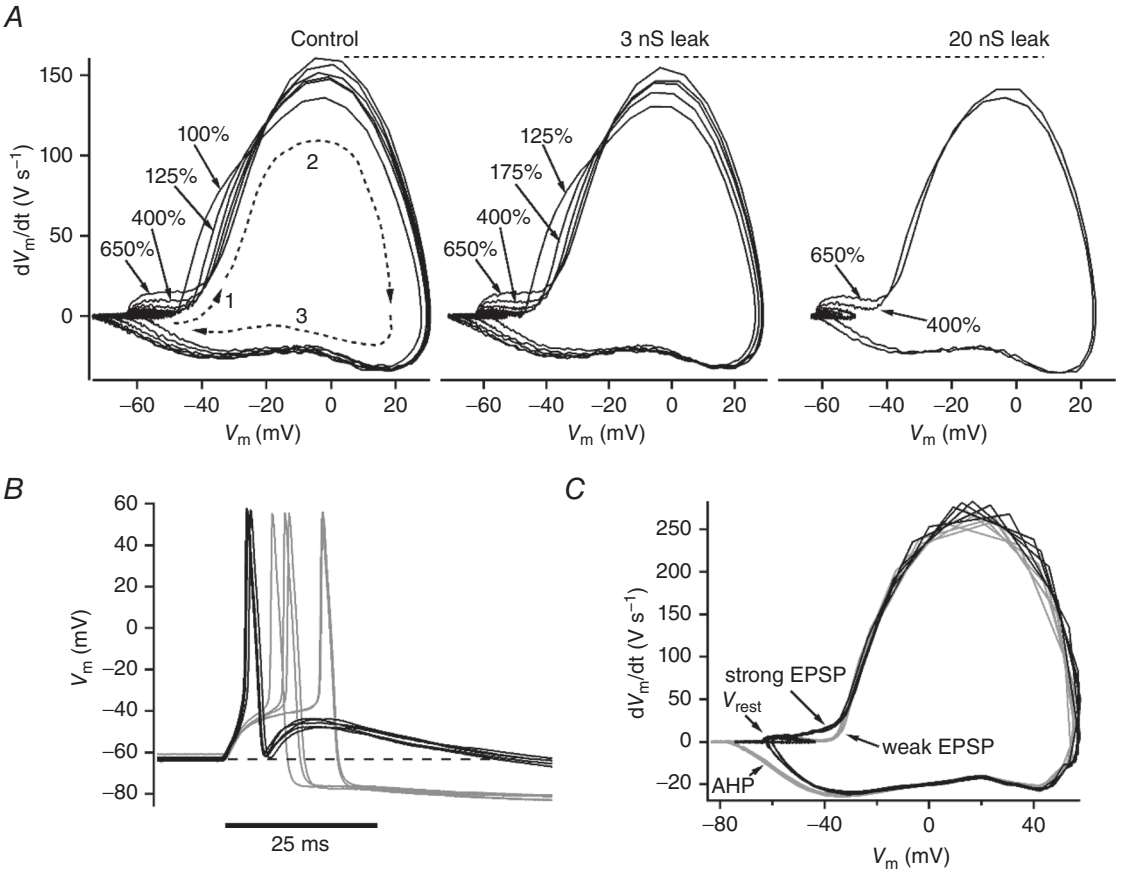

Figure 9. Phase plane trajectories of action potentials driven by virtual nicotinic synapses and biological synapses of different strength
A, families of phase plane trajectories were constructed from spikes driven by virtual EPSPs of defined strength. Data are taken from recordings in Fig. 8. The origin of each cycle begins on the left where $V_m \approx -65$ mV and dV/dt become positive. Dashed arrows in the control cycle denote three phases corresponding to: (1) synaptic excitation; (2) activation of the action potential; and (3) recovery. The strongest EPSPs produce the largest foot at the beginning of the spike cycle, but it never exceeds 25 V s^{-1}. During the fast upstroke (phase 2), dV/dt peaks at about 150 V s^{-1}. At the peak of the action potential, dV_m/dt decreases to 0 V s^{-1} then becomes negative during repolarization. Spikes elicited by the weakest EPSPs have the strongest AHP, which brings the cycle to its most negative voltage at the left of the *x*-axis. Upon adding 3 and 20 nS of g_{leak} the basic shape of the phase plane plots is conserved. However, peak dV_m/dt is reduced (the straight horizontal dashed line marks the peak dV_m/dt of control responses). *B*, examples from the isolated intact superior cervical ganglion of spikes elicited by strong primary EPSPs (black traces) and weaker EPSPs that are barely suprathreshold (grey traces). *C*, phase plane plots of the spikes in (*B*) are similar to those studied in cell culture with virtual synapses (*A*). Differences between spikes driven by strong and weak synapses were clearest at the origin of the cycle where strong EPSPs produce a small foot of about 20 V s^{-1} and at the end of the cycle where weak EPSPs did less to deform the AHP and allow it to reach more nagative values of V_m. AHP, afterhyperpolarization.

Bratton *et al.* 2010). Our results confirm their observation that weak EPSPs reduce peak *dV/dt* during the action potential and shift *dV/dt* to more negative potentials during the AHP. In addition, the peak *dV/dt* of 125 V s^{-1} seen in their data is consistent with the presence of leak damage.

Temporal summation and the impact of g_{leak} upon synaptic gain

The long duration of EPSPs recorded from SCG neurons with patch electrodes implies that temporal summation can occur at long intervals. One can quantitate the magnitude of this effect by measuring the temporal window of summation (t_{sum}). In the original synaptic gain theory, t_{sum} was defined as the maximum interval during which two subthreshold EPSPs of defined strength could summate to initiate an action potential (Karila & Horn, 2000). To measure t_{sum}, we implemented a binary search routine that systematically varied the interval between pairs of virtual EPSPs (Fig. 10). For this particular experiment, synaptic strength was set to 90% thresh-g_{syn}. As can be seen, the EPSPs are well over 100 ms in duration and t_{sum} is close to 90 ms. On average, $t_{sum} = 86.6 \pm 4.1$ ms ($n = 7$). In the t_{sum} experiments, there was no sign of supralinear summation between EPSPs, consistent with the experiments using ZAP stimuli that failed to detect resonance (Fig. 2*B*).

In addition to lowering synaptic strength (Fig. 8), introduction of a leak conductance should reduce t_{sum} and the synaptic gain resulting from the summation of secondary EPSPs. To test this prediction we measured synaptic gain by stimulating neurons with a 40 s periodic dynamic clamp command template that encoded one primary synapse at 300% thresh-g_{syn} and eight secondary synapses at 90% thresh-g_{syn}. The periodic template was designed to mimic presynaptic activity in baroreceptor entrained preganglionic neurons involved in blood pressure regulation (see Methods). The average f_{pre} was 1 Hz for each synapse and the heart rate was 5 Hz with a 20% active duty cycle for presynaptic activity. Figure 11*A* illustrates a 4 s segment from one of these experiments, with the g_{syn} template at the bottom and four trials above with 0–20 nS of added g_{leak}. The V_m recordings show that the most spikes were triggered in the absence of g_{leak} and that adding g_{leak} selectively occluded the spikes driven by secondary EPSPs. During the entire 40 s trial, 41 action potentials originated from the primary synapse and were unaffected by the g_{leak} (Fig. 11*B*). Under control conditions 56 additional action potentials were driven by summation of secondary EPSPs and these spikes were progressively eliminated with introduction of increasing g_{leak} (Fig. 11*C*). Under control conditions mean synaptic gain was 2.44 ± 0.06 ($n = 17$), which was significantly reduced by g_{leak} (3 nS: 1.95 ± 0.05; 10 nS: 1.29 ± 0.05; 20 nS: 1.00 ± 0.02, $P < 0.001$, ANOVA) (Fig. 11*D*). When the control synaptic gain data were broken down in terms of firing dynamics, there was no difference in gain between neurons whose firing dynamics belonged to class 1 (2.61 ± 0.01, $n = 3$), class 2 (2.56 ± 0.06, $n = 4$) or class 3 (2.34 ± 0.09, $n = 10$).

Discussion

We have examined how a leak conductance modulates the intrinsic excitability of sympathetic SCG neurons and the consequences for physiological integration of nicotinic EPSPs. The results provide evidence that synaptic amplification in mammalian sympathetic ganglia may cause a 2.5-fold increase in activity generated by spinal preganglionic neurons. The data also show that similar levels of synaptic amplification can be generated by neurons that differ in their intrinsic excitability. Using the dynamic clamp then revealed how adding a small leak conductance can profoundly alter cellular firing dynamics and synaptic integration. Such effects could prove important in the context of physiological leak channels modulated by metabotropic signalling pathways and they explain the

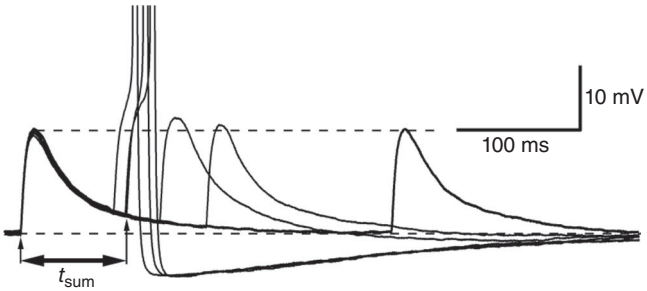

Figure 10. The window of summation for subthreshold virtual nicotinic EPSPs
The temporal window for synaptic summation was measured by varying the interval between pairs of virtual EPSPs whose strength was set to 90% threshold-g_{syn}. Six trials are superimposed in this recording from a dissociated superior cervical ganglion neuron. t_{sum} is the longest interval where summation triggers an action potential. In this cell the virtual EPSPs were longer than 100 ms and $t_{sum} \approx 90$ mS. When the second EPSP in a trial was evoked at intervals $> t_{sum}$, it added linearly to the first EPSP.

disparities between previous observations made with different experimental preparations and intracellular recording methods.

Firing dynamics and channel expression in dissociated superior cervical ganglion neurons

Although Hodgkin's classification scheme for firing dynamics has not been applied to sympathetic neurons until now, earlier work did examine *f–I* relations in SCG neurons from rats of different ages, grown under different conditions. These whole cell patch clamp recordings reveal a remarkable conservation of firing dynamics over a range of conditions.

In the present study, rat sympathetic neurons dissociated from 12 to 15 day pups were maintained for several days in medium with serum and NGF. Plots of *f–I* curves (Fig. 1) revealed that 18% of neurons displayed class 1 firing dynamics, 36% were class 2 and 46% were class 3.

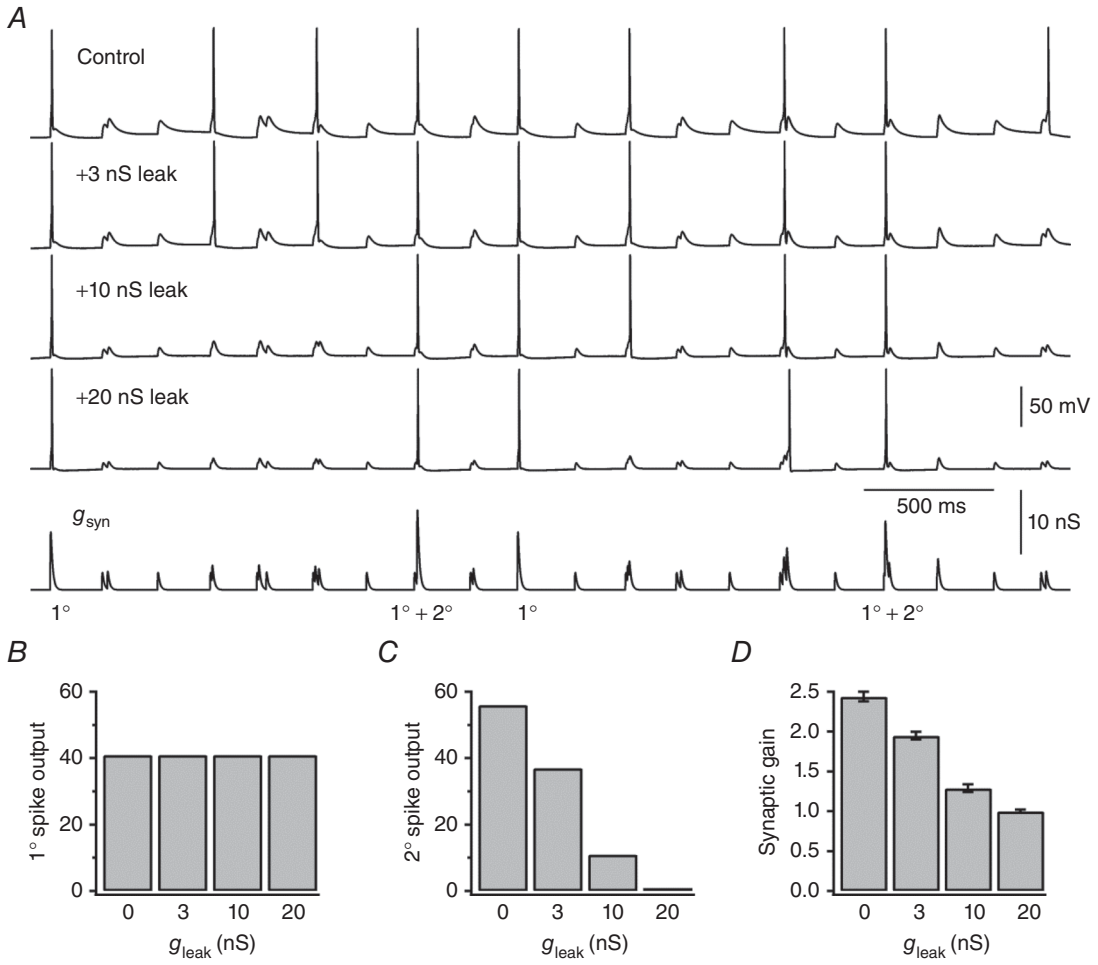

Figure 11. Shunting inhibition by g_{leak} reduces synaptic gain by selectively occluding summation between secondary nicotinic EPSPs
A, identical 4 s segments from longer 40 s trials used to measure synaptic gain in dissociated superior cervical ganglion neurons. The g_{syn} command template (bottom trace), was used to drive the dynamic clamp. It is a periodic combination of events designed to reflect baroreceptor modulated synaptic activity in sympathetic muscle vasoconstrictor neurons (see Methods). The template mimics convergence between one strong primary nicotinic synapse and eight weak secondary nicotinic synapses, each firing at an average rate of 1 Hz. The model produces bursts of synaptic activity that correspond to the cardiac cycle. Under control conditions (top trace), postsynaptic spikes are generated during some, but not all, cardiac cycles and some spikes arise from primary (1°) EPSPs while others arise through summation of secondary (2°) EPSPs. When the trials were repeated after addition of 3–20 nS g_{leak}, a progressive reduction of postsynaptic output resulted from the failure of 2° EPSPs to generate spikes. *B*, counts of 1° spikes for the entire 40 s trial were unaltered by adding g_{leak}. *C*, counts of 2°spikes for the entire 40 s trial showed that they accounted for more than half of the cell's firing, hence a synaptic gain >2. Secondary spike output was reduced after addition of 3 nS g_{leak} and eliminated by 20 nS g_{leak}. *D*, grouped data from 17 neurons show that an average synaptic gain of 2.44 can be reduced to a gain of 1.00 by progressive introduction of g_{leak}.

Nearly identical results were found when neonatal rat SCG neurons (E21–P1) were grown with serum and NGF (Malin & Nerbonne, 2000). These authors classified 25% of cells as tonic, 32% as adapting and 43% as phasic, which resembles our grouping of classes 1, 2 and 3. However, the focus of Malin & Nerbonne (2000) was upon the A-type K^+ current (I_A). They observed cellular heterogeneity in the kinetics and density of I_A. Expression of a dominant negative mutant $K_v4.2$ channel suppressed a fast I_A component and shifted firing dynamics so that more adapting class 2 cells (52%) and fewer phasic class 3 (24%) were observed with no change in the proportion of tonic class 1 cells (24%). Cellular heterogeneity in channel expression can therefore regulate the diverse firing dynamics of SCG neurons. This important concept extends to other voltage-gated ion channels.

The M-type K^+ current (I_M) encoded in SCG neurons by the $K_v7.2$ and $K_v7.3$ genes was the first channel shown to regulate sympathetic firing dynamics (Brown & Passmore, 2009). Inhibition of I_M through muscarinic and other metabotropic receptors can convert cells from phasic to tonic firing (Brown & Adams, 1980; Adams *et al.* 1982, 1986). In addition, differences in I_M expression correlate with the firing dynamics of different cell groups (Jia *et al.* 2008). When SCG cells from 4- to 6-week-old rats were grown for <36 h in defined NGF-free medium, 10% were tonic, 54% phasic 2 and 36% phasic 1 – these groups correspond to classes 1, 2 and 3. I_M density was lowest in tonic cells and highest in phasic 1 cells. Interestingly, acute application of NGF produced a rapid partial inhibition of I_M that selectively enhanced firing by tonic cells. It thus becomes clear that rat SCG neurons from neonatal pups (Malin & Nerbonne, 2000), 2-week-old pups (the present study) and young adults (Jia *et al.* 2008) all display the same three classes of excitability in comparable though not identical proportions.

When firing dynamics were compared in neonatal SCG neurons grown with and without NGF (Luther & Birren, 2006), the authors observed that NGF shifted cells from tonic to phasic firing and they implicated inhibition of multiple K^+ conductances. They subsequently reported that TrkA receptor signalling promotes tonic firing while the p75 pathway promotes accommodation and phasic firing (Luther & Birren, 2009*a*). What then is the intrinsic excitability of sympathetic neurons under normal physiological conditions without the influences of tissue culture and of mechanisms that operate during early development? To answer this question, we went to an enzyme-treated preparation of the acutely isolated adult SCG.

Whole cell recordings from intact ganglia

The paravertebral SCG now joins the list of autonomic ganglia where whole cell recording has become feasible through use of enzyme pretreatments, which are needed to break down connective tissue. The list includes the rabbit prevertebral coeliac sympathetic ganglion (Gola & Niel, 1993), mouse prevertebral superior mesenteric ganglion (Skok *et al.* 1998), embryonic chick ciliary ganglion (Zhang *et al.* 1996; Chang & Berg, 1999; Sargent, 2009; Stanchev & Sargent, 2011), guinea pig enteric ganglia (Kunze *et al.* 2000; Rugiero *et al.* 2002) and mouse enteric ganglia (Mao *et al.* 2006; Osorio & Delmas, 2010; Osorio *et al.* 2014). Interestingly, when patch and microelectrode recordings were compared in enteric neurons (Mao *et al.* 2006) the results were similar to the present findings. Neurons that fired tonically in patch recordings had a much lower R_{in} and fired phasically in microelectrode recordings. Not surprisingly, the quality of patch recordings in each preparation far surpasses those made with sharp microelectrodes. Despite this advantage, these preparations have not been as widely adopted as one might expect, presumably because the methods for enzyme application and washing are slow and tedious. In the hope of simplifying the problem, we adapted a method for preparing the SCG from one developed for dorsal root ganglia (Hayar *et al.* 2008). It avoids the lengthy washing of cells with 'fire hose' streams of multiple solutions before recording and may thereby prove easier for others to implement.

It was surprising to find in the intact adult SCG that 71% of neurons displayed class 1 firing, 29% displayed class 2 firing and none displayed class 3 (Fig. 3). This contrasts markedly with microelectrode evidence that 95–100% of SCG neurons are phasic (class 3) and the remainder are tonic (classes 1 and 2) (Wang & McKinnon, 1995; Jobling & Gibbins, 1999). Instead, our results more closely resembled the properties of patch recordings from prevertebral sympathetic neurons in the coeliac ganglion (Gola & Niel, 1993). Another striking feature of patch recordings from SCG neurons was the duration of primary and secondary nicotinic EPSPs (Fig. 4), which were almost an order of magnitude longer in duration than EPSPs recorded with microelectrodes (McLachlan *et al.* 1997; Rimmer & Horn, 2010). EPSP duration becomes particularly significant when considering temporal summation during the low frequency presynaptic activity that occurs physiologically in this system. Although we cannot explain the absence of class 3 neurons in patch recordings from the adult SCG, the prominence of cells with class 1 and class 2 firing indicates that such behaviour cannot be simply ascribed to tissue culture. Having found that the firing dynamics observed in culture are also expressed in the intact adult ganglion, we proceeded to examine synaptic integration using dynamic clamp.

Modulation of firing dynamics and synaptic gain by leak channels

Given our earlier discussion on modulation of firing dynamics by several voltage-dependent K^+ conductances,

it should not be too surprising that manipulation of leak channels can also transform excitability. Indeed the principle of conversion between firing states has already been established in spinal sensory neurons and cortical pyramidal neurons through the elegant combination of experimental and modelling methods (Prescott *et al.* 2008*a*,*b*). Here we focused on g_{leak} because it provided the most probable hypothesis to explain the disparity between patch and microelectrode recordings from SCG neurons.

We observed that non-depolarizing shunts of 3–20 nS transformed all class 1 and class 2 SCG neurons to class 3 firing dynamics similar to that seen with microelectrodes. For example, the *I–V* relations shown in Fig. 6 for a class 2 neuron with a 10 nS shunt closely resemble the records in fig. 2(B,C) of McLachlan *et al.* (1997). Shunts of this magnitude are consistent with reported values for R_{in}, which we convert to conductance to facilitate discussion. In patch recordings from cells in culture and intact ganglia, input conductances are in the order of 2–2.5 nS. This contrasts with the lowest input conductance values from microelectrode recordings, which are in the order of 4–5 nS and the highest reported values in the range 20–50 nS (Adams & Harper, 1995). Based on these data, we estimate that high-quality microelectrode impalements introduce a shunt most commonly in the order of 3–10 nS. We also conclude that damage accounts for the disparity in firing dynamics between microelectrode and patch electrode recordings. Finding that negative leaks could transform the firing of some neurons in the opposite direction, from class 3 towards class 1 (Fig. 7*A–F*), suggests that variation in background g_{leak} may influence the cellular distribution of firing classes even when recorded with patch electrodes. However, the immutability of other neurons tested with negative leaks (Fig. 7*G*) implies that the diversity of neuronal firing dynamics is physiological rather than a simple consequence of variable recording damage.

Having established that the firing dynamics of SCG neurons were more diverse than previously accepted, it was surprising to find that the consequences for synaptic amplification were minimal. Synaptic gain, when tested with the same periodic template of virtual synaptic activity was 2.61 ± 0.01 in class 1 neurons ($n = 3$), 2.56 ± 0.06 in class 2 neurons ($n = 4$) and 2.34 ± 0.09 in class 3 neurons ($n = 10$) with none of the differences being significant. The simplest explanation for this similarity is the low level of firing in the presynaptic template. Type 1 dynamics would make a difference if cells were subjected to a constant barrage of numerous small EPSPs (Prescott *et al.* 2008*b*) that caused persistent depolarization similar to that observed with current pulses used to construct *f–I* curves. However, physiological levels of preganglionic activity are low and in some cases entrained to the cardiac cycle through baroreceptors (McAllen & Malpas, 1997; Janig, 2006). Action potential generation by subthreshold inputs therefore depends on the transient depolarization by two or more weak EPSPs within the window of summation. At this juncture, it should also be noted that the excitability of the three cell classes did differ in terms of thresh-g_{syn}, which was significantly lower in class 1 neurons than class 3 neurons, with class 2 in the middle (Fig. 5). In all synaptic gain measurements, dynamic clamp command templates were scaled to the same relative strength based on measurements of each cell's thresh-g_{syn}. At present it remains unknown whether the number and strength of physiological synapses converging on cells in the intact SCG are the same for neurons that express different firing dynamics. This leaves open the possibility that specialized cell types within the ganglion have different gain profiles tuned to their specific targets.

The present experiments also illuminate the limitations of *in vivo* intracellular recording with microelectrodes. Our analysis of leak damage shows how shunts having magnitudes similar to those introduced by microelectrodes reduce the strength of virtual nicotinic synapses (Fig. 8) and occlude the impact of secondary nicotinic synapses (Fig. 11*A–C*), resulting in the loss of synaptic gain (Fig. 11*D*). With regard to the integrative role of paravertebral ganglia, a view has emerged from microelectrode recordings that these ganglia behave simply as relays of activity carried by strong primary synapses (McLachlan, 2003). The results presented here support the alternative hypothesis that weak secondary synapses can substantially increase action potential output.

Synaptic amplification posits a more active role than previously envisioned for paravertebral ganglia in processing the outflow from the spinal sympathetic circuitry. What then is the significance of ganglionic gain in light of the idea that sympathetic hyperactivity may act as a driver of human essential hypertension (Joyner *et al.* 2008; Esler, 2010)? Our results suggest that therapeutic targeting of secondary nicotinic synapses on sympathetic neurons that control blood pressure might provide a means for lowering blood pressure without the negative side effects caused by non-selective ganglionic blockade. High-resolution synaptic physiology made possible by patch electrode recording from intact paravertebral sympathetic ganglia may also open doors to re-examine the role of non-nicotinic and non-cholinergic mechanisms in regulating postganglionic activity in sympathetic neurons that control vascular tone (Janig, 2005; Morris *et al.* 2005) and other autonomic functions.

References

Adams PR, Brown DA & Constanti A (1982). Pharmacological inhibition of the M-current. *J Physiol* **332**, 223–262.

Adams DJ & Harper AA (1995). Electrophysiological properties of autonomic ganglion neurons. In *Autonomic Ganglia*, ed. McLachlan EM, pp. 153–212. Harwood Academic Publishers, Luxembourg.

Adams PR, Jones SW, Pennefather P, Brown DA, Koch C & Lancaster B (1986). Slow synaptic transmission in frog sympathetic ganglia. *J Exp Biol* **124**, 259–285.

Bratton B, Davies P, Janig W & McAllen R (2010). Ganglionic transmission in a vasomotor pathway studied *in vivo*. *J Physiol* **588**, 1647–1659.

Brown DA & Adams PR (1980). Muscarinic suppression of a novel voltage-sensitive K^+ current in a vertebrate neurone. *Nature* **283**, 673–676.

Brown DA & Passmore GM (2009). Neural *KCNQ* (Kv7) channels. *Br J Pharmacol* **156**, 1185–1195.

Cassell JF, Clark AL & McLachlan EM (1986). Characteristics of phasic and tonic sympathetic ganglion cells of the guinea-pig. *J Physiol* **372**, 457–483.

Chang KT & Berg DK (1999). Nicotinic acetylcholine receptors containing $\alpha 7$ subunits are required for reliable synaptic transmission *in situ*. *J Neurosci* **19**, 3701–3710.

Derkach VA, Selyanko AA & Skok VI (1983). Acetylcholine-induced current fluctuations and fast excitatory post-synaptic currents in rabbit sympathetic neurones. *J Physiol* **336**, 511–526.

Drummond GB (2009). Reporting ethical matters in *The Journal of Physiology*: standards and advice. *J Physiol* **587**, 713–719.

Erulkar SD & Woodward JK (1968). Intracellular recording from mammalian superior cervical ganglion *in situ*. *J Physiol* **199**, 189–203.

Esler M (2010). Sympathetic nervous activation in essential hypertension: commonly neglected as a therapeutic target, usually ignored as a drug side effect. *Hypertension* **55**, 1090–1091.

Galvan M & Sedlmeir C (1984). Outward currents in voltage-clamped rat sympathetic neurones. *J Physiol* **356**, 115–133.

Gola M & Niel JP (1993). Electrical and integrative properties of rabbit sympathetic neurones re-evaluated by patch clamping non-dissociated cells. *J Physiol* **460**, 327–349.

Hayar A, Gu C & Al-Chaer ED (2008). An improved method for patch clamp recording and calcium imaging of neurons in the intact dorsal root ganglion in rats. *J Neurosci Methods* **173**, 74–82.

Hille B (2001). *Ion Channels of Excitable Membranes*, 3rd edn. Sinauer Associates, Sunderland, MA.

Hodgkin AL (1948). The local electric changes associated with repetitive action in a non-medullated axon. *J Physiol* **107**, 165–181.

Horn JP & Kullmann PH (2007). Dynamic clamp analysis of synaptic integration in sympathetic ganglia. *Neirofiziologiia* **39**, 423–429.

Ivanov A (1991). Pattern of ongoing activity in rat superior cervical ganglion neurons projecting to a specific target. *J Auton Nerv Syst* **32**, 77–79.

Ivanov A & Purves D (1989). Ongoing electrical activity of superior cervical ganglion cells in mammals of different size. *J Comp Neurol* **284**, 398–404.

Izhikevich E (2007). *Dynamical Systems in Neuroscience: The Geometry of Excitability and Bursting*. MIT Press, Cambridge, MA.

Janig W (2005). Non-nicotinic transmission in autonomic ganglia revisited – an important physiological function? *J Physiol* **566**, 1–2.

Janig W (2006). *The Integrative Action of the Autonomic Nervous System*. Cambridge University Press, Cambridge.

Jia Z, Bei J, Rodat-Despoix L, Liu B, Jia Q, Delmas P & Zhang H (2008). NGF inhibits M/KCNQ currents and selectively alters neuronal excitability in subsets of sympathetic neurons depending on their M/KCNQ current background. *J Gen Physiol* **131**, 575–587.

Jobling P & Gibbins IL (1999). Electrophysiological and morphological diversity of mouse sympathetic neurons. *J Neurophysiol* **82**, 2747–2764.

Joyner MJ, Charkoudian N & Wallin BG (2008). A sympathetic view of the sympathetic nervous system and human blood pressure regulation. *Exp Physiol* **93**, 715–724.

Karila P & Horn JP (2000). Secondary nicotinic synapses on sympathetic B neurons and their putative role in ganglionic amplification of activity. *J Neurosci* **20**, 908–918.

Keast JR, McLachlan EM & Meckler RL (1993). Relation between electrophysiological class and neuropeptide content of guinea pig sympathetic prevertebral neurons. *J Neurophysiol* **69**, 384–394.

Kullmann PH & Horn JP (2006). Excitatory muscarinic modulation strengthens virtual nicotinic synapses on sympathetic neurons and thereby enhances synaptic gain. *J Neurophysiol* **96**, 3104–3113.

Kullmann PH & Horn JP (2010*a*). Homeostatic regulation of M-current modulates synaptic integration in secretomotor, but not vasomotor, sympathetic neurons in the bullfrog. *J Physiol* **588**, 923–938.

Kullmann PH & Horn JP (2010*b*). Vasomotor sympathetic neurons are more excitable than secretomotor sympathetic neurons in bullfrog paravertebral ganglia. *Auton Neurosci* **155**, 19–24.

Kullmann PH, Wheeler DW, Beacom J & Horn JP (2004). Implementation of a fast 16-Bit dynamic clamp using LabVIEW-RT. *J Neurophysiol* **91**, 542–554.

Kunze WA, Clerc N, Furness JB & Gola M (2000). The soma and neurites of primary afferent neurons in the guinea-pig intestine respond differentially to deformation. *J Physiol* **526**, 375–385.

Lamas JA (1998). A hyperpolarization-activated cation current (I_h) contributes to resting membrane potential in rat superior cervical sympathetic neurones. *Pflügers Arch* **436**, 429–435.

Li C & Horn JP (2006). Physiological classification of sympathetic neurons in the rat superior cervical ganglion. *J Neurophysiol* **95**, 187–195.

Luther JA & Birren SJ (2006). Nerve growth factor decreases potassium currents and alters repetitive firing in rat sympathetic neurons. *J Neurophysiol* **96**, 946–958.

Luther JA & Birren SJ (2009*a*). Neurotrophins and target interactions in the development and regulation of sympathetic neuron electrical and synaptic properties. *Auton Neurosci* **151**, 46–60.

Luther JA & Birren SJ (2009*b*). p75 and TrkA signaling regulates sympathetic neuronal firing patterns via differential modulation of voltage-gated currents. *J Neurosci* **29**, 5411–5424.

Macefield VG, Wallin BG & Vallbo AB (1994). The discharge behaviour of single vasoconstrictor motoneurones in human muscle nerves. *J Physiol* **481**, 799–809.

Malin SA & Nerbonne JM (2000). Elimination of the fast transient in superior cervical ganglion neurons with expression of KV4.2W362F: molecular dissection of I_A. *J Neurosci* **20**, 5191–5199.

Malin SA & Nerbonne JM (2002). Delayed rectifier K^+ currents, I_K, are encoded by Kv2 α-subunits and regulate tonic firing in mammalian sympathetic neurons. *J Neurosci* **22**, 10094–10105.

Mao Y, Wang B & Kunze W (2006). Characterization of myenteric sensory neurons in the mouse small intestine. *J Neurophysiol* **96**, 998–1010.

McAllen RM & Malpas SC (1997). Sympathetic burst activity: characteristics and significance. *Clin Exp Pharmacol Physiol* **24**, 791–799.

McLachlan EM (2003). Transmission of signals through sympathetic ganglia – modulation, integration or simply distribution? *Acta Physiol Scand* **177**, 227–235.

McLachlan EM, Davies PJ, Habler HJ & Jamieson J (1997). On-going and reflex synaptic events in rat superior cervical ganglion cells. *J Physiol* **501**, 165–181.

McLachlan EM, Habler HJ, Jamieson J & Davies PJ (1998). Analysis of the periodicity of synaptic events in neurones in the superior cervical ganglion of anaesthetized rats. *J Physiol* **511**(Pt 2), 461–478.

Morris JL, Gibbins IL & Jobling P (2005). Post-stimulus potentiation of transmission in pelvic ganglia enhances sympathetic dilatation of guinea-pig uterine artery *in vitro*. *J Physiol* **566**, 189–203.

Osorio N & Delmas P (2010). Patch clamp recording from enteric neurons *in situ*. *Nat Protoc* **6**, 15–27.

Osorio N, Korogod S & Delmas P (2014). Specialized functions of Nav1.5 and Nav1.9 channels in electrogenesis of myenteric neurons in intact mouse ganglia. *J Neurosci* **34**, 5233–5244.

Prescott SA, De Koninck Y & Sejnowski TJ (2008a). Biophysical basis for three distinct dynamical mechanisms of action potential initiation. *PLoS Comput Biol* **4**, e1000198.

Prescott SA, Ratte S, De Koninck Y & Sejnowski TJ (2008b). Pyramidal neurons switch from integrators in vitro to resonators under in vivo-like conditions. *J Neurophysiol* **100**, 3030–3042.

Prinz AA, Bucher D & Marder E (2004). Similar network activity from disparate circuit parameters. *Nat Neurosci* **7**, 1345–1352.

Purves D, Rubin E, Snider WD & Lichtman J (1986). Relation of animal size to convergence, divergence, and neuronal number in peripheral sympathetic pathways. *J Neurosci* **6**, 158–163.

Rimmer K & Horn JP (2010). Weak and straddling secondary nicotinic synapses can drive firing in rat sympathetic neurons and thereby contribute to ganglionic amplification. *Front Neurol* **1**, 130.

Rinzel J & Ermentrout GB (1989). Analysis of neural excitability and oscillations. In *Methods in Neuronal Modeling*, ed. Koch C & Segev I, pp. 135–169. MIT Press, Cambridge, MA.

Rugiero F, Gola M, Kunze WA, Reynaud JC, Furness JB & Clerc N (2002). Analysis of whole-cell currents by patch clamp of guinea-pig myenteric neurones in intact ganglia. *J Physiol* **538**, 447–463.

Sacchi O, Rossi ML, Canella R & Fesce R (2006). Synaptic and somatic effects of axotomy in the intact, innervated rat sympathetic neuron. *J Neurophysiol* **95**, 2832–2844.

Sargent PB (2009). Nicotinic receptors concentrated in the subsynaptic membrane do not contribute significantly to synaptic currents at an embryonic synapse in the chicken ciliary ganglion. *J Neurosci* **29**, 3749–3759.

Schobesberger H, Wheeler DW & Horn JP (2000). A model for pleiotropic muscarinic potentiation of fast synaptic transmission. *J Neurophysiol* **83**, 1912–1923.

Skok VI, Farrugia G, Ermilov LG, Miller SM & Szurszewski JH (1998). Patch-clamp recordings of membrane currents evoked during natural synaptic activity in sympathetic neurons. *Neuroscience* **87**, 509–517.

Skok VI & Ivanov AY (1983). What is the ongoing activity of sympathetic neurons? *J Auton Nerv Syst* **7**, 263–270.

Springer MG (2013). Modulation of synaptic amplification in sympathetic ganglia. In *PhD Dissertation*, pp. 131. University of Pittsburgh.

Stanchev D & Sargent PB (2011). α7-Containing and non-α7-containing nicotinic receptors respond differently to spillover of acetylcholine. *J Neurosci* **31**, 14920–14930.

Tucker KR, Huertas MA, Horn JP, Canavier CC & Levitan ES (2012). Pacemaker rate and depolarization block in nigral dopamine neurons: a somatic sodium channel balancing act. *J Neurosci* **32**, 14519–14531.

Wang HS & McKinnon D (1995). Potassium currents in rat prevertebral and paravertebral sympathetic neurones: control of firing properties. *J Physiol* **485**, 319–335.

Weems WA & Szurszewski JH (1978). An intracellular analysis of some intrinsic factors controlling neural output from inferior mesenteric ganglion of guinea pigs. *J Neurophysiol* **41**, 305–321.

Wheeler DW, Kullmann PH & Horn JP (2004). Estimating use-dependent synaptic gain in autonomic ganglia by computational simulation and dynamic-clamp analysis. *J Neurophysiol* **92**, 2659–2671.

Zhang ZW, Coggan JS & Berg DK (1996). Synaptic currents generated by neuronal acetylcholine receptors sensitive to α-bungarotoxin. *Neuron* **17**, 1231–1240.

Additional information

Competing interests

None of the authors have competing interests

Author contributions

M.G.S. designed and conducted the experiments in cell culture. P.H.M.K. designed and conducted the experiments on whole ganglia. J.P.H. participated in the design and implementation of all experiments. All authors participated in the data analysis. M.G.S. drafted initial versions of the manuscript, P.H.M.K. drafted sections pertaining to his experiments and J.P.H. wrote the final manuscript and made the final figures together with M.G.S. and P.H.M.K.

Funding

This work was initiated with support from NIH grant NS21065 (J.P.H.) and completed with development funds from the University of Pittsburgh School of Medicine.

Acknowledgements

The authors thank Mr James A. Schiela and Dr Kristine M. Sikora for expert technical support.